CHALMERS
UNIVERSITY OF TECHNOLOGY

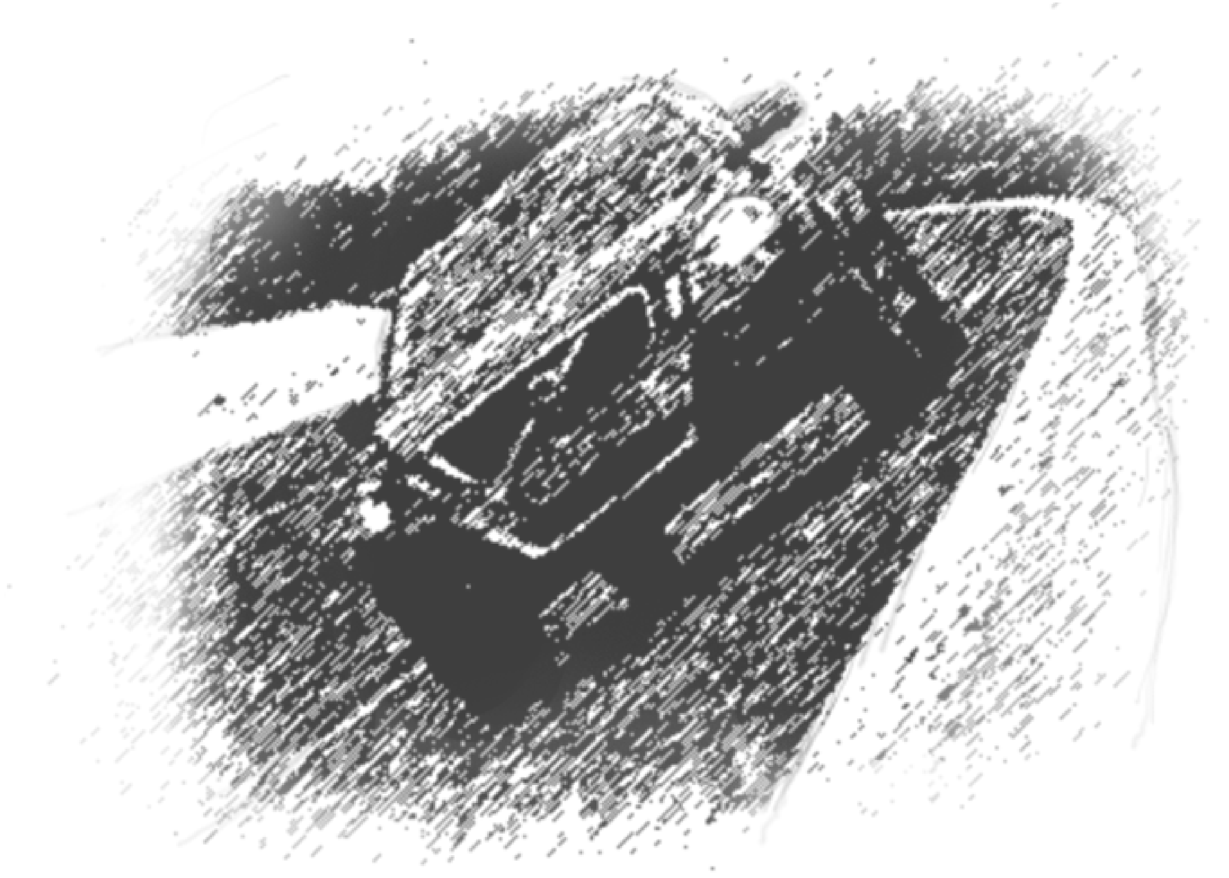

Asymmetry Mitigation by Steering

Modelling and Robust Vehicle Steering Control through EPS

Master's thesis in Systems, Control and Mechatronics / Automotive Engineering

CHRISTOS MARINOS
KONSTANTINOS-EKTOR KARYOTAKIS

Department of Electrical Engineering
CHALMERS UNIVERSITY OF TECHNOLOGY
Gothenburg, Sweden 2019

MASTER'S THESIS 2019:EENX30

Asymmetry Mitigation by Steering

Modelling and Robust Vehicle Steering Control through EPS

CHRISTOS MARINOS

KONSTANTINOS-EKTOR KARYOTAKIS

Department of Electrical Engineering
Division of Systems and Control
CHALMERS UNIVERSITY OF TECHNOLOGY
Gothenburg, Sweden 2019

Asymmetry Mitigation by Steering
Modelling and Robust Vehicle Steering Control through EPS
CHRISTOS MARINOS
KONSTANTINOS-EKTOR KARYOTAKIS

Supervisor and Examiner: Balázs Adam Kulcsár, Electrical Engineering
Industry Supervisor: Carl-Johan Hall, Volvo Cars

Master's Thesis 2019:EENX30
Department of Electrical Engineering
Division of Systems and Control
Chalmers University of Technology
SE-412 96 Gothenburg
Telephone +46 31 772 1000

Cover: High speed driving sketch on superelevated road. Original image courtesy of Volvo Cars

Typeset in LaTeX
Gothenburg, Sweden 2019

Asymmetry Mitigation by Steering
Modelling and Robust Vehicle Steering Control through EPS
CHRISTOS MARINOS
KONSTANTINOS-EKTOR KARYOTAKIS
Department of Electrical Engineering
Chalmers University of Technology

Abstract

This thesis is conducted on behalf of Chalmers University of Technology in collaboration with Volvo Car Corporation. The goal of this thesis was the compensation of road and vehicle asymmetries by utilizing the enhanced capabilities coming with an EPS system. The main idea behind this project was the development of a driver-assistance function providing extra torque when needed, to mitigate unwanted steering and make for a more comfortable driving experience. This work's main contribution is first, a linear steering system model, and second, robust control utilization to overlay compensation torque through the EPS.

Effects such as side winds and road banking can cause short-term unwanted steering, while vehicle asymmetries are known to cause long-term vehicle drift, which the driver has to correct to maintain a straight path. First, a linear model was formulated in order to capture such phenomena, and give a straightforward control synthesis. A 2-mass approximation of the steering system is presented, where the rack got enhanced to carry the effects of the systems around it. This model was then combined with a linear bicycle model to couple vehicle with steering dynamics. Compared to a more accurate, but complex, non-linear model in CarMaker, the developed model shows a good approximation, with reduced computational cost.

To obtain the anticipated performance of the closed-loop system, a model-based, state feedback control strategy is designed. Furthermore, a robust control approach to deal with the perturbations caused by parametric uncertainties is formulated. The robust controller is then updated to include reference tracking. In the end, a comparison between the control strategies is presented, both for pure disturbance rejection as well as achievable reference tracking. Robust control scheme shows to be of higher adaptation capability in a wider assumption and scenario range, as well as better overall performance.

Keywords: robust, steering, EPS, asymmetry, model-based, control, disturbance, rejection.

Acknowledgements

We would like to thank first of all our thesis advisor Balazs Kulcsar of the Department of Electrical Engineering for his guidance and support throughout this project. He consistently encouraged us to take our own initiative, but also steered us in the right direction whenever he thought needed.

We would also like to thank the Steering Department of Volvo Cars. We had been given the needed hardware and software, as well as a suitable workplace to complete our thesis in a comfortable manner. We are also especially grateful to our industry supervisor Carl-Johan Häll. He has always greeted us with positiveness, whenever we needed support. Moreover, he made sure that any administrative issues were quickly resolved, and that we had a smooth integration in the team.

We would also like to acknowledge Mathias Lidberg of the Department of Mechanics and Maritime Sciences for his valuable input in choosing the correct modeling approach.

Christos Marinos, Gothenburg, May 2019
Konstantinos-Ektor Karyotakis, Gothenburg, May 2019

Contents

List of Abbreviations and Symbols

Abbreviations

EPS	Electronic Power Steering
HPS	Hydraulic Power Steering
C.G. P	Centre of Gravity Point
NSP	Neutral Steering Point
AC	Aerodynamic Center
ECU	Electronic Control Unit
EPSc	Column Electronic Power Steering
EPSdp	Dual Pinion Electronic Power Steering
EPSapa	Axis Parallel Electronic Power Steering
PID	Proportional Integral Derivative controller
LQR	Linear Quadratic Regulator
LQI	Linear Quadratic Integral
CARE	Control Algebraic Riccati Equation
SISO	Single Input Single Output
LFT	Linear Fractional Transformation
DoF	Degree(s) of Freedom

Symbols

Bicycle Model:

α Banking Angle

ψ Yaw Angle

$\dot{\psi}$ Yaw Rate or Velocity

β Body Side Slip Angle

u Longitudinal Vehicle Speed

v Lateral Vehicle Speed

V Total Vehicle Speed

F_{y1} Front Axle Lateral Force

F_{y2} Rear Axle Lateral Force

α_1 Front Tyre Slip Angle

α_2 Rear Tyre Slip Angle

δ Road Wheel Angle

m Vehicle Mass

I_z Moment of Inertia about the Vehicle's Vertical Axis

l_1 Distance from the C.G. to the Front Axle

l_2 Distance from the C.G. to the Rear Axle

C_1 Front Axle Cornering Stiffness

C_2 Rear Axle Cornering Stiffness

Steering System:

T_h Driver Torque

T_m Electric Motor Torque

T_o Overlay Motor Torque

T_{tb} Torsion Bar Torque

F_r Tie-rod Force

θ_s Steering Wheel Angle

J_s Steering Column Moment of Inertia

B_s Steering Column Damping

K_s Steering Column Rotational Stiffness

x_r Rack Position

M_r Rack Mass

B_r Rack Damping

K_r Rack Stiffness

J_m Electric Motor Moment of Inertia

B_m Electric Motor Damping

K_m Electric Motor Rotational Stiffness

g_m Electric Motor Transmission Ratio

r_p Pinion Radius

r_m Motor Effective Radius

r_k Steering Arm Length

t_m Mechanical Trail

t_p Pneumatic Trail

List of Figures

1

Introduction

During the past decades, research in the automotive industry has progressed. Much effort has been made in improving the vehicles' attributes of safety, comfort, and performance, while special need for reduction of their environmental impact has risen. To meet these goals, vehicles have become smarter and more complex. Their level of automation has increased, while the trend has been for more electrical systems to be added and/or replace the existing mechanical ones.

The steering system is the main input for the lateral control of a vehicle, and is therefore a perfect candidate to follow these trends. In order to reduce the effort a driver has to exert to steer, power-assist systems have been introduced. For years, the standard has been the hydraulic power-assist steering (HPAS/HPS) system, but is being gradually replaced by the electric power-assist steering (EPAS/EPS) system. The main advantages of a change to EPS comes from the reduction of power and emissions, and the increased functionality they provide, which makes for advances in the areas of safety, ride comfort, and driver-assist [1].

These attributes of the EPS system have opened the path to research on new functions and capabilities. Phenomena that produce unwanted steering and compromise the occupants' safety can be mitigated, while on the same time ride comfort is improved. These phenomena are mostly associated with their effect on the lateral control of the vehicle. Although their governing physics are known [2], there has not been much effort in research on devising a mitigation strategy. As for the automotive industry, there has only been but recently that the suppliers of the EPS systems have begun offering such compensation functions, but only in their premium models [3]. In most cases however, the driver is still solely responsible to compensate for them. Concluding, there is the need to analyze such phenomena and devise a suitable mitigation strategy for their physical effect on the vehicle. This had been a major concern motivating this work.

Practically, with the EPS the driver could be completely bypassed. This opens also the path to a high degree of automation. There is though a fine line between how much these systems interfere and how much is needed. There is presented the risk of creating a false perception of an overly safe environment. The driver by using their senses interprets the environment and the vehicle's behavior, and judges how to take action. In the case of the steering system there are two important measures which the driver uses in that manner, the steering feel, and the road feel. Road feel can be explained as what the driver interprets from the vibrations he senses from the steering wheel, which connects to the road profile. Steering feel is the torque feel on the steering wheel based on the steering wheel angle [4], which gives the vehicle's limits to the driver. EPS systems though have produced problems with taking too much away from the driver, presenting risks of false perception [5]. However, the feel characteristics have not been investigated in detail in this thesis, but should be accounted for in future work.

2

Background

2.1 Vehicle Motion by Disturbance

Generally, a vehicle moving freely in the horizontal plane is subject to external lateral disturbance, which induces unwanted motion. As a categorization property for the disturbances, the disturbance time application was chosen. In other words, how long the disturbance is acting on the vehicle. Two main categories are identified, as short-term and long-term. For the short-term effects, the most common lateral force disturbances come from road banking and side winds. As for the long-term effects, properties of the vehicle itself are the main contributors, like tyre and suspension misalignments.

In [2], the effects of such disturbances on a moving vehicle are studied. Different response is expected, based on the application point of the force and the centre of gravity position (C.G. P). Two more points of interest are defined: the neutral steering point (NSP) and the aerodynamic center (AC). In the case of the NSP, it is the acting point of the resultant force of the tyre lateral forces. Its location depends on the vehicle's internal stability. As for the AC, it is solely dependent on the aerodynamic shape of the object.

In Figure 2.1 the above analysis can be seen. In most cases, a vehicle is performing as understeered, so the left side of the figure is the most relevant, while the middle refers to a neutral steered and the right to an oversteered vehicle.

2.1.1 Road Banking

In order to avoid excessive amounts of water resting on the road surface, the road exhibits a small lateral slope starting from its centerline and ending to both sides of the road. This road geometry is most commonly referred to as "crown". Normal crown of roads is usually in the range of $1 - 2$ % [6].

In curves, to help the vehicles when cornering, the outer edge is superelavated. By introducing road superelavation, the cornering forces are reduced by an induced body force due to gravity. This helps the vehicle stay in lane. However, when roads are poorly made, a negative superelavation can occur resulting in the opposite effect. A maximum superelevation of 7 % can be found in road design.

In this report, the term "banking" will be used in a general manner to describe the negative

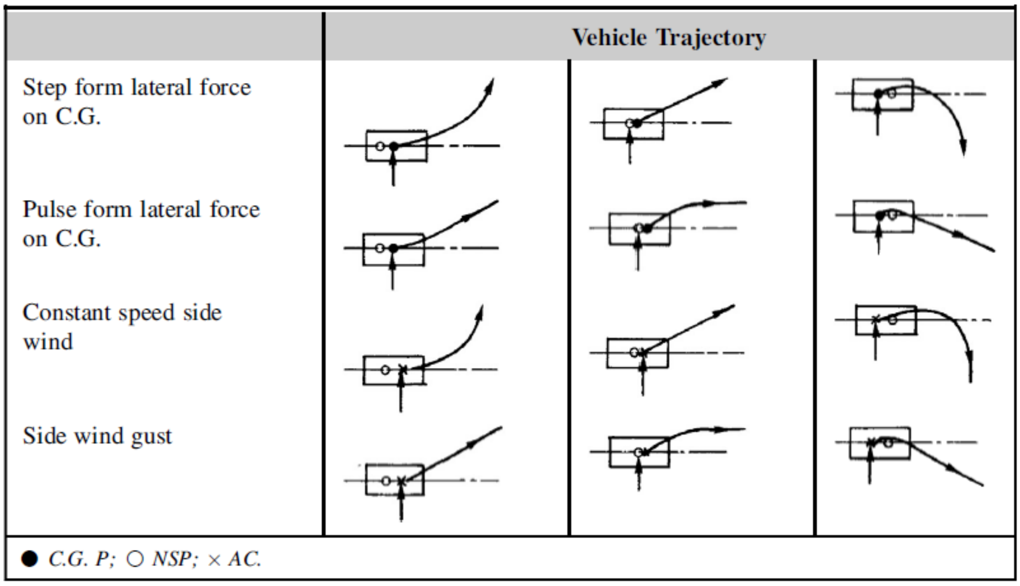

Figure 2.1: Vehicle Motion Subjected to Lateral Disturbance, adopted from [2]

effect a lateral road slope induces, which can be found either because of normal crown or other effects associated with poor road conditions.

In Figure 2.2, such a lateral force can be seen. The force due to road banking is exerted on the C.G and is given by

$$F_b = mg \sin\alpha \tag{2.1}$$

while the lateral slope of the road is usually described in percentage, as per

$$s_r = \tan\alpha = \frac{\Delta h}{\Delta w} \tag{2.2}$$

where α is the road bank angle, Δh the road's height, and Δw the road's lateral length.

It should be mentioned that the upper bounds of α found in road design lie well within the small angles approximation region. Thus, the statement that $\sin\alpha \approx \tan\alpha \approx \alpha$, can be used in the above equations.

2.2 Steering system

A common configuration of a modern steering system most usually includes the following components: steering wheel, steering column, steering gear (pinion), rack, steering actuator (power-assist system), and two tie rods [1].

The input to the system is given by the driver from the steering wheel. Their commands are transferred through the other components causing their kinematic motion. The rotation of the steering wheel causes the rotation of the steering column and the steering gear, which in turn translates the circular motion into linear movement of the rack. Then, the rack's movement, translated via the tie rods and the steering arm, forces the wheels to

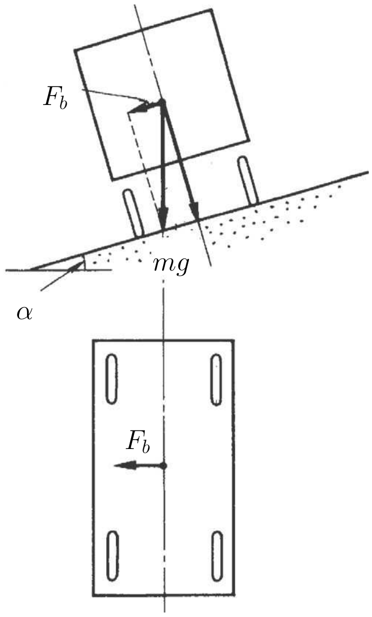

Figure 2.2: Lateral Force due to Bank Angle, adopted from [2]

rotate around their steering (kingpin) axis. A schematic of a typical steering system can be seen in Fig 2.3.

The steering actuator or power-assist system has become a standard component for some years now. Its major mission is to help the driver steer, by applying extra boost. Most vehicles still use HPS for its proved performance through the years [8]. However, the benefits which EPS brings have already been briefly discussed and as it is the actuator of choice, its basics will be covered.

There are 4 main parts of an EPS: 1) a servo-electric motor, 2) an electronic control unit (ECU), 3) a torque sensor, and 4) mechanical power transmission to the steering system. Depending on the power demand, the actuator can be placed at different points. This could be the column (EPSc) for smaller vehicles, or the rack. At the rack it can be either with a separate second pinion (EPSdp), or belt-driven on a parallel axis (EPSapa). Part of a steering system with EPSapa can be seen on Fig 2.4.

2.2.1 Modeling

In literature, there has been investigation on modeling of the steering system, with Pfeffer and Harrer's work [1] to be of the most famous ones. From a system point of view, the steering system can be approximated with one set of equations for every subsystem it includes: one for the column, one for the rack, one for the suspension and wheels, and one for the electric motor with its transmission system. Inclusion of the kinematics and inertial phenomena must be accounted for, while relevant simplifications can be made in each subsystem. In most of the cases, each subsystem is approximated to a simple mass-damper-spring system.

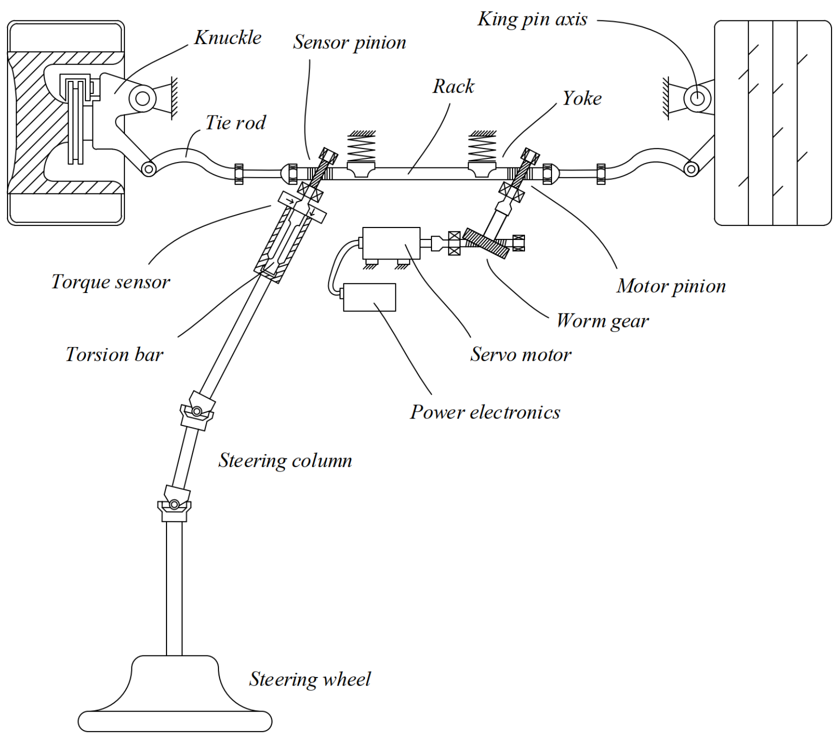

Figure 2.3: Schematic of an EPSdp steering system, adopted from [7]

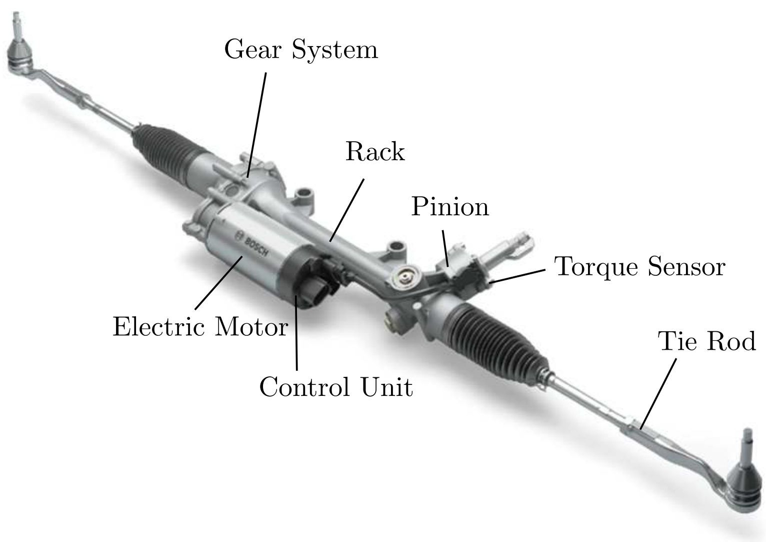

Figure 2.4: Steering system with EPSapa, reworked from [3]

Measured inputs to the system can be the torque or angle at the steering wheel, provided by the torsion bar sensor and an encoder on the steering wheel respectively. The EPS also provides the motor's torque and angle. Moreover, there is usually an encoder on the pinion to measure this angle as well, which can be directly related by the pinion's ratio to the rack position.

The motor of the EPS boosts the driver's input depending both on their request and the current vehicle speed. From the sensed torque, the motor's torque is taken from a third order curve, while as the speed increases the slope is reduced to avoid big steering movements, for safety reasons. That kind of relation can be seen in Fig 2.5.

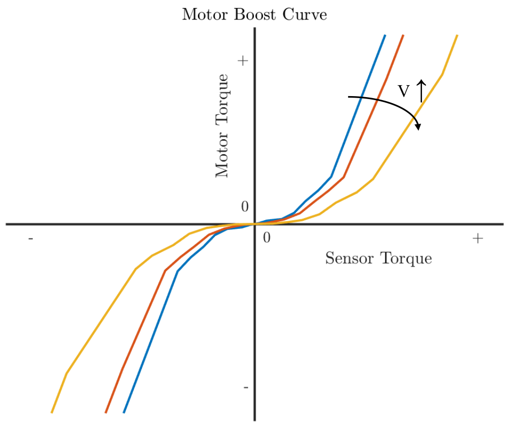

Figure 2.5: Motor Boost Curve

2.3 Proportional Integral Control

PI controller is based on the following equation:

$$u(t) = K_p\ e(t) + K_I \int_0^t e(\tau) d\tau \tag{2.3}$$

where $u(t)$ is the control input and $e(t)$ is the control error ($e = r - y$). The control input $u(t)$ is a sum of two terms, the proportional (P-term) and the integral term (I-term). The controller parameter k is a vector of two terms as well. The proportional gain k_p and the integral gain k_I.

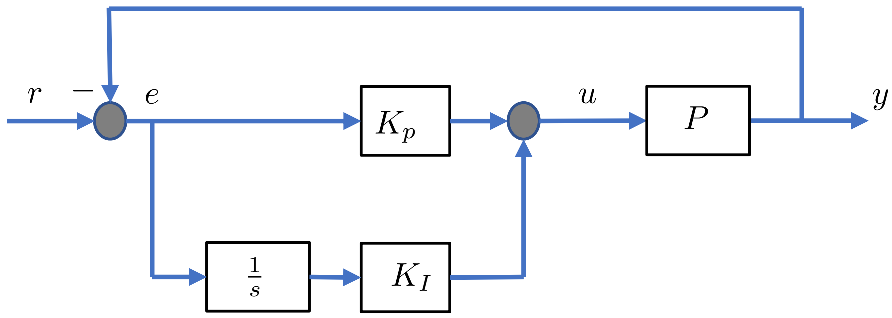

Figure 2.6: Proportional Integral Controller - Closed Loop

The error $e(t)$ is formulated by the difference between the desired or reference value $r(t)$ and the closed loop measured value $y(t)$, as shown in Figure 2.6. By introducing integral action, it is guaranteed that the reference agrees with the measured signal in steady state [9].

2.4 Linear Quadratic Regulator Control

The Linear Quadratic Regulator (LQR) Controller is a model-based control strategy, which uses the states of a linear model to provide a control output that is used as control input to the system, formulating a closed-loop. First, consider the following LTI system

$$\dot{x}(t) = Ax(t) + Bu(t), \quad x(0) = x_0 \tag{2.4}$$

the formulated control law will have the form

$$u(t) = -Kx(t)$$

where the optimal control $u(t)$ is a function of the states, a negative feedback.

The goal when using optimal control is to find a control law that will satisfy the optimal criteria of the system. Optimal control can be achieved by using the Euler Lagrange equation, by deriving the functions that the cost functional, a function of state and control variables, is stationary i.e.minimized [10]. The cost functional J has the form

$$J = \frac{1}{2}\int_0^{\infty} \underbrace{\left(x^T(t)Q_x x(t) + u^T(t)Q_u u(t)\right)}_{V(x,u)} dt = \frac{1}{2}\int_0^{\infty} V(x,u)dt \tag{2.5}$$

where $Q_x \in \mathbb{R}^{n\times n}, Q_x^T = Q_x \geq 0$, $Q_u \in \mathbb{R}^{n\times p}, Q_u^T = Q_u \geq 0$.

By using $J^* = \min_{u(t)} J$ the closed-loop poles can be chosen accordingly. For obtaining an optimal feedback $u^*(t)$, the Euler-Lagrange equation is used. First, the Euler-Lagrange equation is formulated

$$L(x,u,\lambda) = V + \lambda^T(t)(Ax(t) + Bu(t) - \dot{x}(t)) = \tag{2.6}$$

$$x^T(t)Q_x x(t) + u^T(t)Q_u u(t) + \lambda^T(t)(Ax(t) + Bu(t) - \dot{x}(t))$$

where $\lambda(t)$ is the co-state variable and V is the term of the cost functional.

The conditions for solving the Lagrangian equation and obtaining an optimal control law in this case are

$$\frac{\theta L}{\theta x(t)} - \frac{d}{dt}\frac{\theta L}{\theta \dot{x}(t)} = 0 \tag{2.7}$$

$$\frac{\theta L}{\theta u(t)} - \frac{d}{dt}\frac{\theta L}{\theta \dot{u}(t)} = 0 \tag{2.8}$$

$$\frac{\theta L}{\theta \lambda(t)} - \frac{d}{dt}\frac{\theta L}{\theta \dot{\lambda}(t)} = 0 \tag{2.9}$$

Thus, by solving the conditions above, the following results are derived. The optimal control input has the form

$$u^*(t) = -Q_u B^T \lambda(t) \tag{2.10}$$

and the state space equation ends up as

$$\dot{x}(t) = Ax(t) - BQ_u^{-1}B^T\lambda(t) \tag{2.11}$$

while the co-state variable $\lambda(t)$ is

$$\dot{\lambda}(t) = -Q_x x(t) - A^T\lambda(t) \tag{2.12}$$

By taking into consideration that the co-state $\lambda(t)$ is proportional to the state variable $x(t)$ as $\lambda^*(t) = P(t)x(t)$, where $P(t)$ is a time-varying matrix, equation (2.12) can be written as

$$\dot{\lambda}(t) = -\dot{P}(t)x(t) + P(t)\dot{x}(t) \tag{2.13}$$

and by substituting with the equation (2.11), the following equation is derived

$$(\dot{P}(t) + P(t)A + A^T P(t) + Q_x - P(t)BQ_u^{-1}B^T P(t))x(t) = 0 \tag{2.14}$$

For ensuring that the equation is true for non zero states of $x(t)$, the matrix $P(t)$ has to satisfy the equation

$$\dot{P}(t) + P(t)A + A^T P(t) + Q_x = P(t)BQ_u^{-1}B^T P(t) \tag{2.15}$$

which is known as the Differential Riccati Equation (DRE).

The steady-state solution of the Differential Riccati Equation can then be obtained.

$$\bar{P}A + A^T\bar{P} + Q_x = \bar{P}BQ_u^{-1}B^T\bar{P} \tag{2.16}$$

Note that by using $\bar{}$ notation, the steady state value of the variable is used [11].

This equation is also known as the Control Algebraic Riccati Equation (CARE). By using CARE and the state-space matrices, the steady state value of $\bar{P}$ can be derived. The optimal control will then have the form

$$u^*(t) = -Q_u^{-1}B^T\bar{P}x^*(t) = -\bar{K}x^*(t)$$

where $\bar{K}$ is known as the Linear Quadratic (LQ) gain [12].

The optimal control input $u^*(t)$ is then fed back to the system, as depicted in Figure 2.7 and the closed loop system has the form

$$\dot{x}(t) = (A - BK)x(t) \tag{2.17}$$

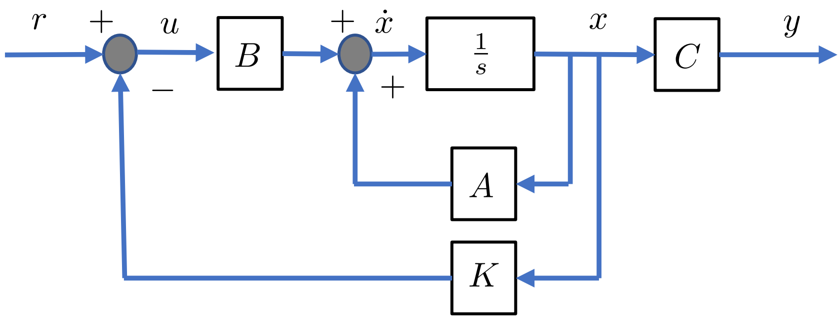

Figure 2.7: LQR Controller - Closed Loop

2.5 Linear Quadratic Integral control

Linear Quadratic Integral control is an approach for reference tracking, by integrating the tracking error $e(t) = r(t) - y(t))$. The formulation of the control gain is similar to the Linear Quadratic Regulator, but with the difference of introducing an extra integral state, or states, which have the form:

$$z(t) = \int_0^t (r(t) - y(t))dt$$

The augmented State Space System form is shown in Equation 2.18

$$\begin{bmatrix} \dot{x} \\ \dot{z} \end{bmatrix} = \begin{bmatrix} A & 0 \\ C & 0 \end{bmatrix} \begin{bmatrix} x \\ z \end{bmatrix} + \begin{bmatrix} B \\ 0 \end{bmatrix} u + \begin{bmatrix} K_r \\ -I \end{bmatrix} r \tag{2.18}$$

The control input $u(t)$, similarly to the Linear Quadratic Regulator implementation, will have the form:

$$u = -\begin{bmatrix} K_x & K_I \end{bmatrix} \begin{bmatrix} x \\ z \end{bmatrix}$$

The goal while using the Linear Quadratic Integral Controller is to derive an optimal control law for minimizing the cost functional

$$J = \frac{1}{2} \int_0^\infty \underbrace{\left(x^T(t) Q_{x_I} x(t) + u^T(t) Q_{u_I} u(t)\right)}_{V(x,u)} dt = \frac{1}{2} \int_0^\infty V(x,u)dt \tag{2.19}$$

where $Q_{x_I} \in \mathbb{R}^{n \times n}, Q_{x_I}^T = Q_{x_I} \geq 0$, $Q_{u_I} \in \mathbb{R}^{n \times p}, Q_{u_I}^T = Q_{u_I} \geq 0$ [13].

The procedure is similar with Linear Quadratic Regulator procedure, where a gain K can be derived by solving the CARE

$$\bar{P}A + A^T\bar{P} + Q_x = \bar{P}BQ_u^{-1}B^T\bar{P}$$

The closed loop system with the feedback control input $u(t)$ is depicted in Figure 2.8.

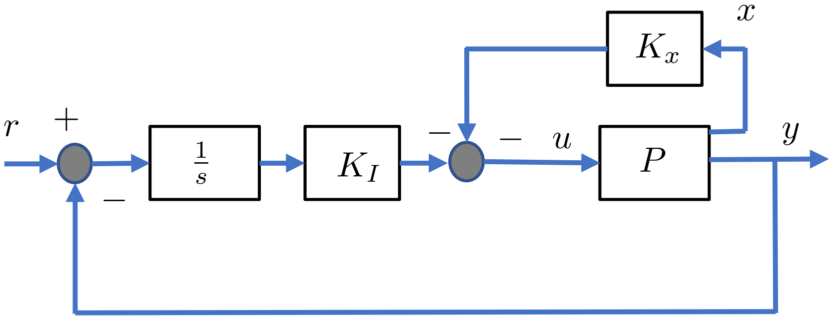

Figure 2.8: Linear Quadratic Integral Controller - Closed Loop

2.6 Robust Control

2.6.1 System Norms

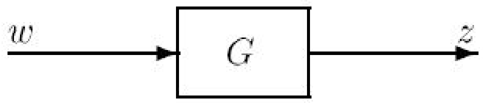

Figure 2.9: System G

System norms are a tool for evaluation of a system's performance. Assume a Single Input, Single Output ($SISO$) system with an impulse response $g(t)$, represented by a stable transfer function G, as shown in Figure 2.9. The system norms are used for describing the reaction between the output z of the system and the input information w, considering that variable w is given. Two types of system norms are used to describe the performance of the system, the H_2 and H_∞ norms.

For the H_2 case the Frobenius norm is used and then integration over time. The Frobenius or Euclidean norm is a matrix norm of an $m \times n$ matrix A. It is defined as the square root of the sum of the absolute square of the matrix's elements. It is also equal to the square root of the matrix trace of AA^H, where A^H is the conjugate transpose [14].

Consequently, the H_2 norm of the strictly proper system $G(j\omega)$ would be

$$||G(s)||_2 = \sqrt{\frac{1}{2\pi}\int_{-\infty}^{\infty} tr(G(j\omega)^H G(j\omega)) \quad d\omega}$$

According to Parseval's theorem, the H_2 norm of the system's transfer function is equal to the H_2 norm of the impulse response

$$||G(s)||_2 = ||g(t)||_2 = \sqrt{\frac{1}{2\pi}\int_0^\infty tr(g^T(\tau)g(\tau)) \quad d\tau} \tag{2.20}$$

Equation 2.20 can be also written as

$$||G(s)||_2 = ||g(t)||_2 = \sqrt{\sum_{ij}\int_0^\infty |g_{ij}(\tau)|^2 \quad d\tau}$$

where $g_{ij}(t)$ is the ij'th element of $g(t)$.

This equation can be translated as the 2-norm of the system derived by applying a Dirac delta fuction $\delta(t)$ as input signal.

Regarding the stochastic interpretation of the H_2 norm, by substituting the transfer function with the state space matrices as $G(s) = C(sI - A)^{-1}B$, the H_2 norm would be

$$|||G(s)||_2 = \sqrt{tr(B^TQB)} = \sqrt{tr(CPC^T)}$$

In this interpretation the expected root mean square (rms) value of the output is measured in response to a disturbance signal.

For the $\mathcal{H}_\infty$ norm the singular value is used. The absolute value of the eigenvalues of the matrix A can be used to derive the singular value of the matrix [15]. The singular value of the system G is the induced form of the H_2 norm. The H_∞ norm of the system represents the peak value of the induced form as a function of frequency. It can also be formulated as the magnitude of a closed loop system, which is upper-bounded by a specified value.

$$||G(s)||_\infty = \max_\omega \bar{\sigma}(G(j\omega))$$

Moreover, it can be computed numerically from a state-space realization as the smallest value of γ, such that the Hamiltonian matrix in (2.21) has no eigenvalues on the imaginary axis

$$H = \begin{bmatrix} A + BR^{-1}D^TC & BR^{-1}B^T \\ -C^T(I + DR^{-1}D^T)C & -(A + BR^{-1}D^TC)^T \end{bmatrix} \tag{2.21}$$

It should be noted that the parameter γ is a free parameter.

2.6.2 System Interconnection

In order to meet the performance specifications of the system, the weighted system interconnection is used. The weights are additional information for design and can be either input or output weights as shown in Figure 2.10.

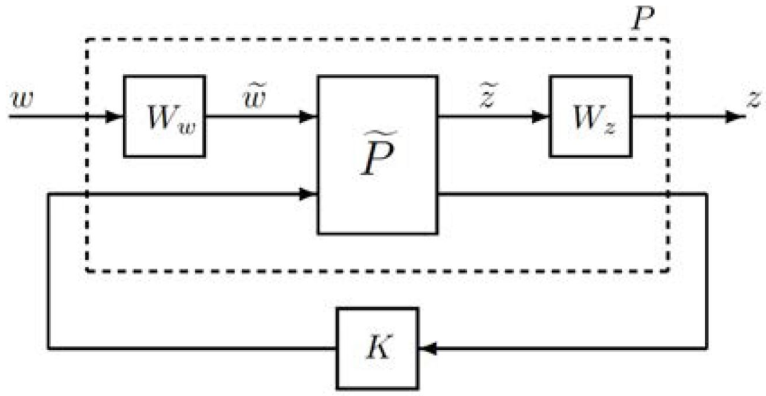

Figure 2.10: PK structure with input and output weights.

As for the weight selection, the input weights are used for $\tilde{w} = W_w w$, where w is a normalized exogenous input. $\tilde{w}$ is a signal shaped in frequency and magnitude by a dynamic weight (transfer function matrix) W_w. Based on the same principal, output weights are used for $\tilde{z} = W_z z$, where W_z is introduced to normalize $\tilde{z}$. The output weight is dependant on frequency.

Considering that a system has a number of weighted inputs u and weighted performance outputs z, the open - loop, weighted interconnected model can be derived. This model is nothing more than the transfer function of the weighted nominal plant. In other words, an augmented, weighted form of the nominal model [16]. The open-loop partition will have the form:

$$\begin{bmatrix} z \\ \upsilon \end{bmatrix} = P \begin{bmatrix} w \\ u \end{bmatrix} \tag{2.22}$$

The outputs of the system are defined as the performance outputs z and the measured outputs υ that are used as controller inputs. As inputs w to the augmented system the following signals are usually considered

1. Disturbance
2. Nominal Plant inputs
3. Noise

The plant P will have the following form

$$P = \begin{bmatrix} P_{11} & P_{12} \\ P_{21} & P_{22} \end{bmatrix} \tag{2.23}$$

Each element of the P matrix represents a transfer function from a specific input to a specific output. For closing the loop between the weighted system and K, the Linear Fractional transformation (LFT) is used. The outputs of the system can be expressed based on the inputs, according to the equations

$$z = P_{11}w + P_{12}u = P_{11}w + P_{12}\upsilon$$

$$\upsilon = P_{21}w + P_{22}K\upsilon \Rightarrow (I - P_{22}K)\upsilon = P_{21}w \tag{2.24}$$

Based on the block models in Figure 2.11 and the I/O equations in 2.24, the closed loop interconnection between the Plant P and the controller K, or else PK structure, has the form

$$N = P_{11}w + P_{12}K(I - P_{22}K)^{-1}v = F_l(P, K) \tag{2.25}$$

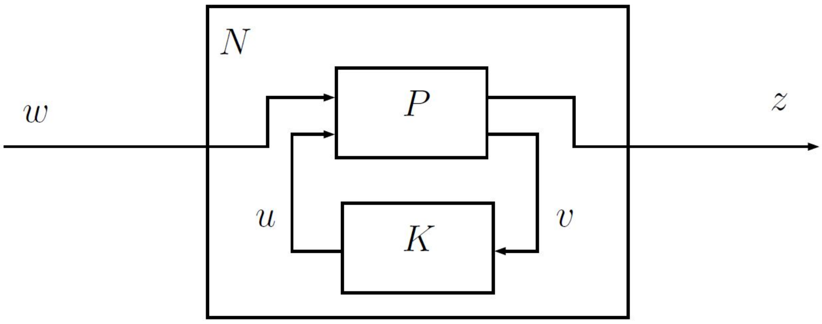

Figure 2.11: NPK structure

2.6.3 Parametric Uncertainty

A control system is called robust, when the performance of the controller is not affected by the differences between the controlled system and the system used to design the controller. These differences can be also referred to as model uncertainties and can have several origins. One form of uncertainty is the parametric uncertainty. The parametric uncertainties represent the differences between the parameters of the controlled model and the model used for the design of the controller and can be caused by multiple reasons, such as non-linearities, sensor noise and approximation mismatch. The parametric uncertainty shows that each parameter is bounded between a region $[\alpha_{min}, \alpha_{max}]$. Consequently, the uncertain parameter set will have the form:

$$x_p = \bar{x}(1 + r_x\Delta) \tag{2.26}$$

where $\bar{x}$ is the mean value, $r_x = (x_{max} - x_{min})/(x_{max} + x_{min})$ the relative uncertainty and Δ is any real scalar satisfying $|\Delta| \leq 1$.

Due to the difficulty of parametric uncertainty modelling, they can be represented as perturbations. Each perturbation is assumed to be stable and normalized as

$$\bar{\sigma}(\Delta_i(j\omega)) \leq 1 \quad \forall\omega \tag{2.27}$$

In order to obtain a controller that is robust, the control problem has to be formulated in an uncertain environment. The form of the system showcased in Figure 2.12 is useful to obtain a controller to compensate for the perturbations caused by the uncertain parameters.

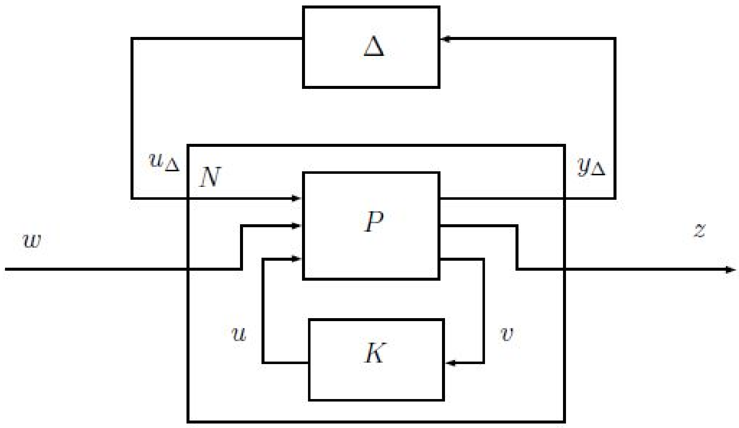

Figure 2.12: General Control Configuration

Alternatively, if the controller is given and the goal is to analyze the uncertain system, the $N\Delta$ structure is used. The perturbation blocks form Δ and the nominal system N is related to P and K by a lower LFT similar as in (2.25). The transfer function from the input w to the performance output z,which is denoted by F ($z = Fw$), is related to N and Δ by an upper LFT equation

$$F_u(N, \Delta) = N_{22} + N_{21}\Delta(I - N_{11}\Delta)^{-1}N_{12} \tag{2.28}$$

The closed-loop system has then the form:

$$\begin{bmatrix} y_\Delta \\ z \end{bmatrix} = \begin{bmatrix} N_{11} & N_{12} \\ N_{21} & N_{22} \end{bmatrix} \begin{bmatrix} u_\Delta \\ w \end{bmatrix} \tag{2.29}$$

The control signals u and v are considered as internal signals and not as inputs to the system.

Finally, the performance of the system is verified by defining some metrics, listed below.

1. **Nominal Stability, NS:** Given the nominal system model G, the controller K stabilizes the closed-nominal loop.
   Verification: The nominal structure is internally stable

2. **Robust Stability, RS:** Given the nominal system model G and model perturbation Δ, the controller K stabilize all perturbed models within Δ
   Validation: Given $||\Delta||_\infty < 1$, *Robust Stability is satisfied if* $||N_{11}||_\infty < 1$

3. **Nominal Performance, NP:** The interconnected structure N satisfies the criteria for Nominal Stability and the performance criteria are met for the nominal plant P.
   Validation: NS is satisfied and $||N_{22}||_\infty < 1$

4. **Robust Performance, RP:** The closed loop system N satisfies the criteria for Robust Stability and all the performance criteria are still met.
   Validation: RS is satisfied and $||N||_\infty \leq 1$

2.6.4 1 Degree of Freedom $\mathcal{H}_\infty$ Controller

The general problem formulation is depicted in Figure 2.13.

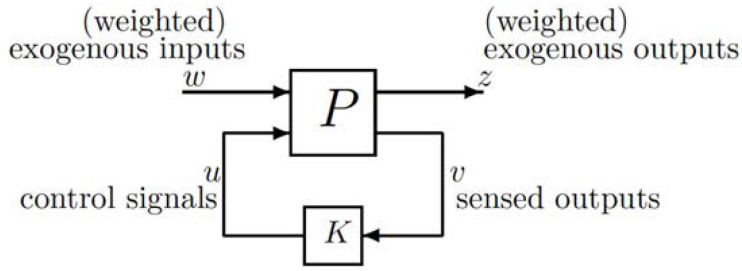

Figure 2.13: General control configuration

The system interconnection of Figure 2.13 is based on the equations

$$\begin{bmatrix} z \\ v \end{bmatrix} = P \begin{bmatrix} w \\ u \end{bmatrix} = \begin{bmatrix} P_{11} & P_{12} \\ P_{21} & P_{22} \end{bmatrix} \begin{bmatrix} w \\ u \end{bmatrix} \tag{2.30}$$

$$u = K(s)v \tag{2.31}$$

where u are the control variables, v are the measured variables, w represent the exogenous signals, such as disturbances and z are the performance outputs, which are to be minimized to obtain the desired control performance.

The performance outputs are connected with the exogenous input signals through equation (2.24). Based on Figure 2.13, the optimal control problem is to find the controllers $K(t)$ which minimizes the closed-loop system

$$||F_l(P,K)||_\infty = \max_\omega \bar{\sigma}(F_l(P,K)(j,\omega)) \tag{2.32}$$

which is the peak of the maximum singular value of the LFT.

Equation (2.32) can be interpreted in time domain as

$$||F_l(P,K)||_\infty = \max_{\omega(t)\neq 0} \frac{||z(t)||_2}{||w(t)||_2}$$

where

$$||z(t)||_2 = \sqrt{\int_0^\infty \sum_i |z_i(t)|^2} \tag{2.33}$$

is the 2-norm of the performance output signal. Similarly, the norm of the exogenous input can be obtained.

As robust control theory requires a very complex methodology to obtain a perfect controller, it is more common and more efficient at the same time to design a sub-optimal controller. The sub-optimal control problem is defined as:

for $\gamma > \gamma_{min}$: *find all stabilizing controllers K(s) such that*

$$||F_l(P,K)||_\infty < \gamma \tag{2.34}$$

If $P(s)$ has the following form in time domain

$$\begin{bmatrix} \dot{x} \\ z \\ \upsilon \end{bmatrix} = \left[\begin{array}{c|cc} A & B_1 & B_2 \\ \hline C_1 & D_{11} & D_{12} \\ C_2 & D_{21} & D_{22} \end{array}\right] \begin{bmatrix} x \\ w \\ u \end{bmatrix} \tag{2.35}$$

Given that the (A, B_2, C_2) model is stable and detectable, then there exists a stabilizing and disturbance rejecting dynamic output feedback controller $K(s)$ such that $||F_l(P,K)||_\infty < \gamma$ if and only if:

1. Obtain a solution to the algebraic Riccati equation $\bar{P}_1 \geq 0$
$$A^T\bar{P}_1 + \bar{P}_1 A + C_1^T C_1 + \bar{P}_1(\gamma^{-2}B_1B_1^T - B_2B_2^T)\bar{P}_1 = 0$$
such that $Re(\lambda(A + (\gamma^{-2}B_1B_1^T - B_2B_2^T)\bar{P}_1)) < 0, \forall i$
2. Obtain a solution to the algebraic Riccati equation $\bar{P}_2 \geq 0$
$$A^T\bar{P}_2 + \bar{P}_2 A + B_1 B_1^T + \bar{P}_2(\gamma^{-2}C_1^TC_1 - C_2^TC_2)\bar{P}_2 = 0$$
such that $Re(\lambda(A + \bar{P}_2(\gamma^{-2}C_1^TC_1 - C_2^TC_2))) < 0, \forall i$
3. $\rho(\bar{P}_1, \bar{P}_2) < \gamma^2$,the spectral radius of $\bar{\lambda}(\bar{P}_1, \bar{P}_2)$ is not larger than γ^2 ; γ attenuation level is ensured.

With these condition a set of controller candidates $K = F_l(K_c, Q)$ are defined, where

$$K_c(s) = \left[\begin{array}{c|cc} A_c & B_{1c}\bar{L} & B_{2c} \\ \hline C_{1c} & 0 & I \\ C_{2c} & I & 0 \end{array}\right] \tag{2.36}$$

$$C_{1c} = -B_2^T\bar{P}_1, \quad \bar{L} = -\bar{P}_2C_2^T, \quad B_{1c} = -(I - \gamma^{-2}\bar{P}_2\bar{P}_1)^{-1}, \quad B_{2c} = -B_{1c}B_2 \quad C_{2c} = -C_2$$
$$A_c = A - (-\frac{1}{\gamma^2}B_1B_1^T + B_2B_2^T)\bar{P}_1 - (I - \gamma^{-2}\bar{P}_2\bar{P}_1)^{-1})\bar{P}_2C_2^TC_2$$

and $Q(s)$ is any stable transfer function that $||Q(s)||_\infty < \gamma$.

The "central" controller will have the form

$$K(s) = K_{c_{11}}(s) = -C_{1c}(sI - A_c)^{-1}B_{1c}\bar{L} \tag{2.37}$$

which has the same number of states as the plant P. The central controller can then be separated into a state estimator and a state feedback, as shown in the equations below [17], [16].

$$\dot{\tilde{x}} = A\tilde{x} + B_1\gamma^{-2}B_1^T\bar{P}_1\tilde{x} + B_2u + B_{1c}\bar{L}(C_2\tilde{x} - y) \tag{2.38}$$
$$u = C_{1c}\tilde{x} \tag{2.39}$$

2.6.5 2 Degree of Freedom $\mathcal{H}_\infty$ Controller

The difference between the 1 Degree of Freedom and 2 Degree of Freedom H_∞ controller is that the input to the controller is not only the measured or feedback variables, but also the reference signal, as shown in Figure 2.14. For example, Figure 2.15 depicts the

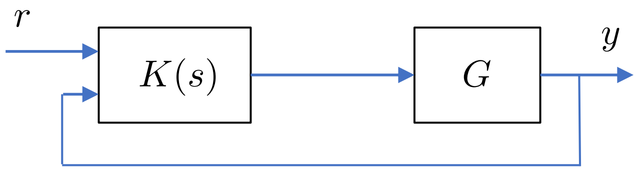

Figure 2.14: General reference tracking feedback control scheme

interconnection between the 2 Degree of Freedom $\mathcal{H}_\infty$ controller and the Plant. The goal

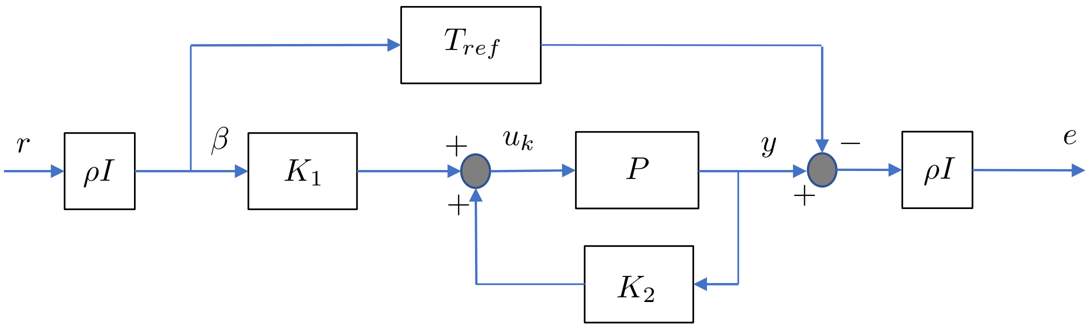

Figure 2.15: 2 Dof H_∞ problem

of the optimal robust control theory is to find a stabilizing controller $K = \begin{bmatrix} K_1 & K_2 \end{bmatrix}$ for the plant P that minimizes the H_∞ norm between the input signals, which in this case are the reference, the control input in the system and the error.

The control input to the nominal plant P, would be

$$u_k = \begin{bmatrix} K_1 & K_2 \end{bmatrix} \begin{bmatrix} \beta \\ y \end{bmatrix} \tag{2.40}$$

where K_1 is the pre-filter, K_2 is the feedback controller, β is the scaled reference, and y are the measurement outputs. If G is the transfer function of the nominal plant P and T_{ref} is the transfer function to obtain the desired reference value, the pre-filter is used with the purpose of

$$||(I - G_s K_2)^{-1} G_s K_1 - T_{ref}||_\infty \leq \gamma \rho^{-2} \tag{2.41}$$

where ρ is a user-defined parameter to adopt to the desired performance criteria.

As for the feedback controller K_2, the same procedure is followed like the previous subsection for obtaining the central controller. The basic difference when designing a 2 degree of freedom controller is the system interconnection between the plant P, the reference signal r and how these parameters would be defined in order to form the closed-loop [17].

2.7 Mean Estimation

When there is the need to estimate the mean and variance from data collection, estimators are used. The probability distribution needs to be known to define a random sample of the population. A random sample is used when the population is too big or the means to gather data are too costly.

Consistent and unbiased estimators of mean and variance are given by (as seen in [18])

$$\hat{\mu} = \frac{1}{n}\sum_{i=1}^{n} x_i \tag{2.42}$$

and

$$\hat{\sigma}^2 = \frac{1}{n-1}\sum_{i=1}^{n} (x_i - \overline{x}) \tag{2.43}$$

where x is the random variable, $\hat{\mu}$ the mean estimator, and n the sample size of the random sample.

Usually in practical applications, the method of choice for estimators comes from the maximum likelihood estimation (MLE). However, the above given equations provide both an unbiased and consistent estimation for the case of a normal (continuous) distribution. The mean equation (2.42) is the same for MLE as well for a normal distribution, but for the variance MLE gives a biased estimator. These estimators ((2.42)-(2.43)) will be used for the long term estimation in 3.9.

Another useful equation is

$$n \geq \left(\frac{Z_{1-\frac{\alpha}{2}}}{d}\right)\sigma^2 \tag{2.44}$$

which gives the lower limit of the required size n of the sample to have an α % percentage confidence interval, for a given acceptable error d and variance σ^2.

3

Methods

3.1 Linear Model

In order to design the controllers, a model is needed. The model needs to be linear and at the same time cover real life in a good extent. That is, to have easy implementation and quick iteration in the design procedure. For the vehicle dynamics part, a linear bicycle model was decided to be used, as it is a very good match for the low dynamics coming from road banking disturbance. It is valid for relative mediocre speeds [19], where this feature is most needed. About the steering system, a model was made based on literature, mainly inspired by [20]. Such a model is needed mainly because the control input utilizes the motor's torque, which in turn influences the whole steering system. Both of the models, along with their coupling, are presented in the coming sections.

3.1.1 Bicycle Model

First, a linear bicycle model is introduced, including the forces applied due to banking. For the linearization, roll effects are ignored, and the vehicle's longitudinal speed u is assumed to be constant ($u \approx V$) so that no influence from the lateral components of the longitudinal forces is regarded. Small angles approximation is also assumed [19] for all the slip angles, i.e. $[\alpha_1, \alpha_2, \beta]$. The approximations used in this case are presented in general form: $\sin\theta \approx \theta$ and $\tan\theta \approx \theta$. A basic bicycle model can be seen on Fig 3.1 and based on it the dynamic equilibrium is built. The velocity vectors are depicted with blue color.

The equations of motion for the linear bicycle model read

$$m(\dot{v} + u\dot{\psi}) = F_{y1} + F_{y2} \tag{3.1}$$

$$I_z\ddot{\psi} = l_1 F_{y1} - l_2 F_{y2} \tag{3.2}$$

with v denoting the lateral velocity in the center of gravity and $\dot{\psi}$ the yaw velocity. The symbol I_z denotes the moment of inertia about the vehicle's vertical axis, and m the vehicle's mass.

The body slip angle β is expressed as

$$\beta = \arctan\left(\frac{v}{u}\right) \approx \frac{v}{V} \tag{3.3}$$

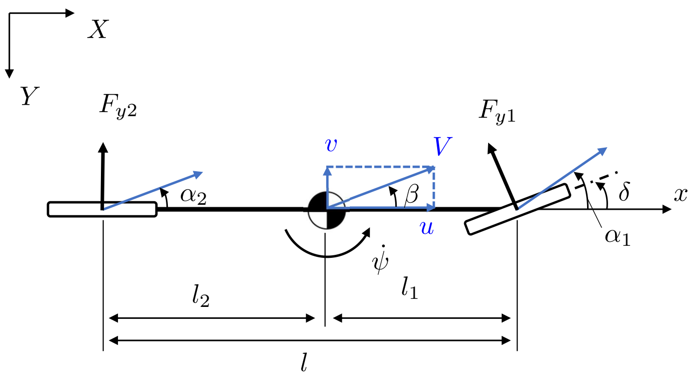

Figure 3.1: Bicycle Model

and will be used instead of v as a state.

The lateral forces are taken by the linear tyre expression

$$F_{y1} = C_1\alpha_1 \tag{3.4}$$
$$F_{y2} = C_2\alpha_2 \tag{3.5}$$

where the tyre slip angles $[\alpha_1, \alpha_2]$ are given as

$$\alpha_1 = \delta - \beta - \frac{l_1\dot{\psi}}{V} \tag{3.6}$$
$$\alpha_2 = -\beta - \frac{l_2\dot{\psi}}{V} \tag{3.7}$$

with δ being the road wheel angle.

By adding the banking force from eq. (2.1) in (3.3), the equations in state space form become

$$\begin{pmatrix} \dot{\beta} \\ \ddot{\psi} \end{pmatrix} = \underbrace{-\begin{pmatrix} \frac{C_1+C_2}{mV} & 1+\frac{C_1l_1-C_2l_2}{mV^2} \\ \frac{C_1l_1-C_2l_2}{I_z} & \frac{C_1l_1^2+C_2l_2^2}{I_zV} \end{pmatrix}}_{A_a} \begin{pmatrix} \beta \\ \dot{\psi} \end{pmatrix} + \underbrace{\begin{pmatrix} \frac{C_1}{mV} \\ \frac{C_1l_1}{I_z} \end{pmatrix}}_{B_a} \delta + \underbrace{\begin{pmatrix} -\frac{g}{V} \\ 0 \end{pmatrix}}_{B_{w_a}} \sin\alpha \tag{3.8}$$

3.1.2 Steering System Model

From the 4 main subsystems which describe the steering system, depending on the wanted inputs and outputs different simplifications can be made. For this work, the column and the rack were decided to be of most importance and all the other subsystems are to be translated into those. That is, the motor and suspension dynamics were decided to be simplified and included into the spring, mass and damping coefficients of the connected subsystem [21], where in both cases is the rack. Following the above, a 2-mass approach of the steering system is used.

As the model is to be used for control purposes, linearization is needed to be made. As in the case of the bicycle model, steady state phenomena need to be captured, while much detail of the dynamics is not needed. The main non-linearities in the steering system come from friction forces. Pfeffer and Harrer [22] have approximated them with some complex mathematical models. The basic idea is that every friction force consists of two parts: a spring force, and a damping force part. The spring part is approximated by an exponential function, while the damping part by a hyperbolic function. Both parts bottom out at the static friction value. However, as this approach overcomplicates the model, it was decided not to use it, but approximate the friction forces with linear expressions instead, as in [20].

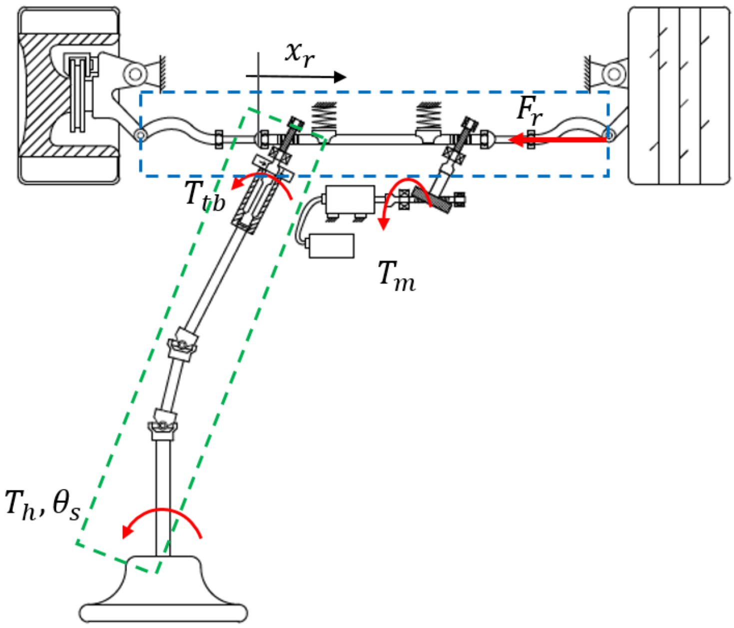

Figure 3.2: Steering System Free Body Diagram, reworked from [7]

In Fig 3.2, a free body diagram of a steering system with EPSdp is shown. The column and the rack are highlighted with green and blue respectively, representing the two main subsystems. In the following equations, the 2-mass system for the steering column and rack are stated

$$J_s\ddot{\theta}_s + B_s\dot{\theta}_s + K_s\theta_s = -T_{tb} + T_h \tag{3.9}$$

$$M_r\ddot{x}_r + B_r\dot{x}_r + K_r x_r = \frac{T_{tb}}{r_p} + g_m\frac{T_m}{r_p} - F_r \tag{3.10}$$

Torsion bar:

$$T_{tb} = K_{tb}\left(\theta_s - \frac{x_r}{r_p}\right) + B_{tb}\left(\dot{\theta}_s - \frac{\dot{x}_r}{r_p}\right) \tag{3.11}$$

T_h, T_{tb}, T_m, F_r represent the applied driver torque, torsion bar torque, electric motor torque, and road forces from the tie rods; θ_s, x_r are the steering wheel angle, and rack position; J_s, B_s, K_s are the steering column inertia, rotational damping, and stiffness; M_r, B_r, K_r are the equivalent rack's mass, damping, and spring coefficient; K_{tb}, B_{tb} are the torsion bar rotational stiffness, and torsion bar rotational damping; r_p is the pinion's radius; g_m is the motor's transmission ratio.

To be noted that for the motor, the same gear radius is assumed as for the pinion. This makes the effective motor radius actually

$$r_m = \frac{r_p}{g_m} \tag{3.12}$$

As for the mass and damping of the rack in (3.10), an equivalent one was chosen by taking into account the servo motor's and suspension interaction

$$M_r = m_r + \frac{J_m}{r_m^2} + \frac{J_{wl}}{r_k^2} \tag{3.13}$$

$$B_r = b_r + \frac{B_m}{r_m^2} + \frac{B_{wl}}{r_k^2} \tag{3.14}$$

where $m_r,\ b_r$ are the actual mass and damping coefficient of the rack, $[J_{wl}, B_{wl}]$ are the moment of inertia and damping of the suspensions and wheels, and r_k is the steering arm length.

3.1.3 Combining the models

The two model, bicycle and steering, connect to each other through the tie rods. The self-aligning torque is the torque around the steering axis caused by the lateral tyre force, and is the main contributor to the tie-rod force, at the speeds where the bicycle model is valid. That is, from about 30 kph and above. At lower speeds, the linear tyre force to slip angle relation (3.4)-(3.5) is not valid anymore. Low-speed phenomena, due to mainly suspension kinematics, increase the tie-rod forces and as they become of similar magnitude to the self-aligning torque, they cannot be ignored anymore. That said, the low-speed region will not be covered.

The forces in the tie rods mainly contain the forces coming from the tyres, and external forces

$$F_r = (F_{y1} + F_e)\zeta \tag{3.15}$$

where F_{y1} is the lateral force in the front axle coming from (3.4), F_e expresses external forces, and ζ is a ratio defined as

$$\zeta = \frac{t_m + t_p}{r_k} \tag{3.16}$$

where t_m is the mechanical trail, and t_p the pneumatic trail.

F_e includes all other phenomena not covered by the tyre cornering forces. These can be forces caused by suspension or tyre asymmetries. For instance tyre plyrat is a common such asymmetry, which causes a small constant force on each tyre caused by the tyre plies. However, as some of these effects can be also included in the cornering stiffness as compliance, F_e will be thus ignored and the cornering stiffness will be regarded as an uncertain parameter later in the controller design (see section 3.7.2). For the ones that cannot be included in the cornering stiffness, as for instance the tyre plyrat force which is approximately constant, a different approach will be presented in section 3.9, as their magnitudes are generally unknown.

Expression (3.15) is actually the translation of the aligning torque from the tyres to the rack. Moreover, the pneumatic trail with linear tyre force expressions can be approximated by the following equation (as seen in [19])

$$t_p \approx \frac{a}{2} \tag{3.17}$$

where a is half the contact length of the tyre, and is expressed by

$$a = a_0\sqrt{F_z/F_{z0}} \tag{3.18}$$

where a_0 is a parameter, F_z the vertical load of the tyre, and F_{z0} is the nominal load.

In addition to the tie-rod forces, the rack's movement is also coupled to the wheels' through their kinematics. The wheel angle can be expressed as a function of rack position or steering wheel angle as

$$\delta = \frac{\theta_s}{r_k} r_p = \frac{x_r}{r_k} \tag{3.19}$$

which connects the bicycle model's input to the steering system states in equation (3.6) and through the front axle lateral force ((3.4),(3.15)) affects the rack (3.10). The complete tie rod force then becomes

$$F_r = C_1\left(\frac{x_r}{r_k} - \beta - \frac{l_1\dot{\psi}}{V}\right)\zeta \tag{3.20}$$

The bicycle model (3.8) is combined to the steering system equations (3.9)-(3.11), through the tie rod force (3.20) and it is presented in matrix form, with state vector $x = \begin{bmatrix}\theta_s & \dot{\theta}_s & x_r & \dot{x}_r & \beta & \dot{\psi}\end{bmatrix}^\intercal$, input $u = \begin{bmatrix}T_h & T_m\end{bmatrix}^\intercal$, output $y = \begin{bmatrix}\theta_s & x_r & T_{tb}\end{bmatrix}^\intercal$, and disturbance $w = \alpha$

The state space of the model is established in the form

$$\begin{cases}\dot{x} & = Ax + Bu + B_w w \\ y & = Cx + Du\end{cases} \tag{3.21}$$

where

$$A = \begin{bmatrix} 0 & 1 & 0 & 0 & 0 & 0 \\ \frac{-K_{tb}}{J_s} & -\frac{B_{tb}+B_s}{J_s} & \frac{K_{tb}}{J_s r_p} & \frac{B_{tb}}{J_s r_p} & 0 & 0 \\ 0 & 0 & 0 & 1 & 0 & 0 \\ \frac{K_{tb}}{M_r r_p} & \frac{B_{tb}}{M_r r_p} & -\frac{K_r r_p^2 + K_{tb}}{M_r r_p^2} - \frac{C_1\zeta}{M_r r_k} & -\frac{B_r r_p^2 + B_{tb}}{M_r r_p^2} & \frac{C_1\zeta}{M_r} & \frac{C_1 l_1 \zeta}{M_r V} \\ 0 & 0 & b_1/r_k & 0 & a_{11} & a_{12} \\ 0 & 0 & b_2/r_k & 0 & a_{21} & a_{22} \end{bmatrix}$$

$$B = \begin{bmatrix} 0 & 0 \\ \frac{1}{J_s} & 0 \\ 0 & 0 \\ 0 & \frac{1}{M_r r_m} \\ 0 & 0 \\ 0 & 0 \end{bmatrix}, \quad B_w = \begin{bmatrix} 0 \\ 0 \\ 0 \\ 0 \\ -\frac{g}{V} \\ 0 \end{bmatrix}, \quad C = I_{6\times 6}, \quad D = 0$$

$[b_1,\ a_{11}..]$ come from the bicycle model matrices $[A_a,\ B_a]$.

3.1.4 Model Frequency Response

The complete nominal plant, including the disturbance, is defined in eq. (3.21). In order to see though the system's behavior as well as the effect of the disturbance separately, the following singular value plot is shown in Fig 3.3. G is the plant with its normal inputs, while G_d depicts the plant with the disturbance as input instead. A first natural frequency can be observed at 2.5 Hz and a second one at 10 Hz. This is a known issue with the inclusion of an EPS instead of HPS [7], coming mainly from the increase in inertia (see equation (3.13)). The outputs yaw rate, and side slip angle exhibit their resonance a bit below 1 Hz [19], making the system prone to excitations around the region $1-2$ Hz. This affects the controller design, as it will be also shown in the coming sections. As for the disturbance, it actually enhances the low frequency region, while after the first natural frequency the response is dampened.

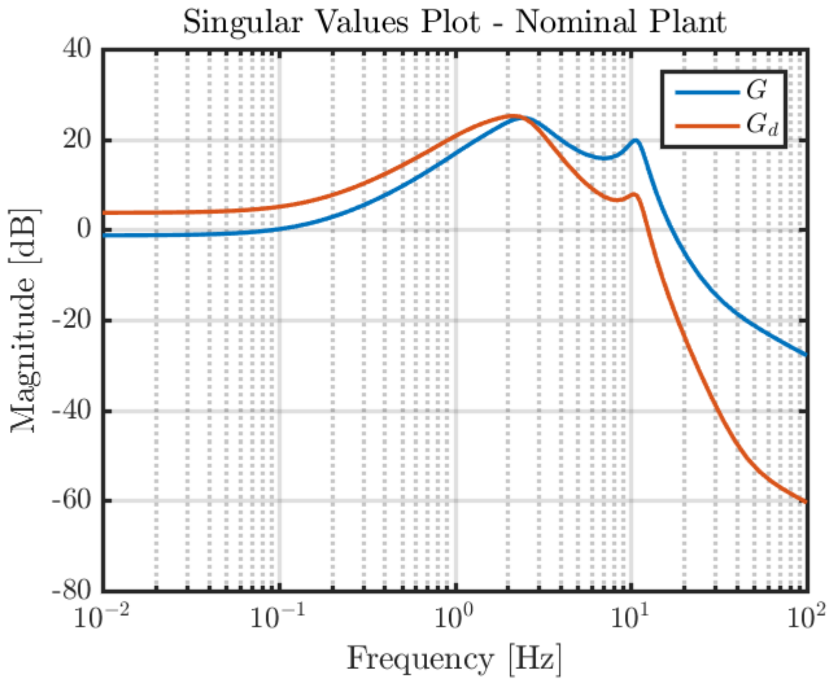

Figure 3.3: Nominal Plant Singular Values

3.2 Electric Power Steering (EPS) System

For this project, the EPS system is used in the closed loop analysis to provide the control input. The control input is basically a torque boost, which can be overlaid over the torque provided by the electric motor to compensate the effects of the disturbance. That is for simplicity of adding extra functions to the EPS, where that extra torque request is limited for safety and power purposes. As seen in (3.22), a maximum of ±1 Nm is assumed for this limitation.

$$|T_o| \leq 1 \tag{3.22}$$

3.3 Simulation

3.3.1 Matlab/Simulink

The Matlab numeric environment was used both for the design and implementation of the 2-mass linear model as well as for the design and tuning of the model-based, state feedback controllers. The graphical programming environment of Simulink was used for the system interconnection, formulation of the closed-loop systems, and simulation of their behavior. Finally, most data figures presented are taken through this software.

3.3.2 CarMaker Software

In order to validate and test the model's and controller's capabilities, the non-linear, high fidelity simulation environment CarMaker was used. CarMaker is a simulation software that provides the opportunity to do office or real-time simulation on a Hardware-in-the-Loop (HIL) test bench for the development and test of complex embedded systems. The general structure of the software consists of the Virtual Vehicle Environment (VVE) and the CarMaker Interface Toolbox (CIT) as shown in Figure 3.4 [23].

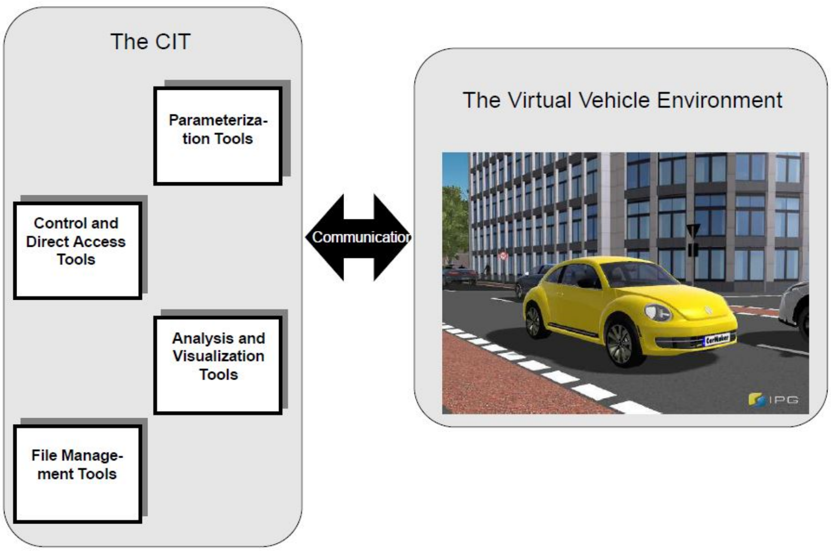

Figure 3.4: CarMaker Software - General Structure

The VVE consists of the virtual representation of the vehicle, the road and the driver. A virtual Vehicle is a modeled representation of a vehicle with a behavior that matches the real world behavior of the vehicle. Different equations, formulas and kinematics combine to make a bigger, multibody system. The model is also parameterized with data from tests and other simulations to better match real life. Moreover, a virtual road is also modelled to represent real road conditions. The road can either be designed from the beginning, by using the toolboxes provided or can be created from using digitized data of an existing road. Finally, there are driver models, and simple manoeuvres, varying from turning the steering wheel to shifting gears.

For most of the cases, the test roads and manoeuvres were created from scratch. For the simulations, CarMaker's coupling environment to Simulink was used. This enabled the direct use of the already built models and controllers from Simulink to CarMaker.

3.4 Linear Quadratic Regulator

The model-based technique followed for the Linear Quadratic Regulator, requires a linear model for designing the controller and obtaining a gain K.

First, the design parameters Q_x, Q_u of the cost functional should be specified. Although in most cases is an arbitrary choice, a general, not so formal, plan has been followed. The matrix Q_x is defined as a $n \times n$ matrix, where n is the number of states of the linear model. For this implementation, the states of yaw rate $\dot{\psi}$ and the steering angle θ_s are penalized. These two states are important for keeping the car in the lane. The Bryson or Inverse Square rule is used for normalizing terms in the cost function, and used as the first tuning step. Then, the normalized state is multiplied with a gain, trying to match the ideal performance.

For obtaining a robust controller, which will be able to compensate any disturbance applied and manage to get yaw rate to the desired value, which is zero in this case, a "cheap" control energy should be achieved. The control energy is cheap if for the control input gain $Q_u = \rho I$ and $0 < \rho << 1$. In general, the control input is penalized with a smaller gain than the states, in order to achieve a robust control performance.

The weights used for the implementation of the controller are presented, focusing explicitly on the yaw rate. For ensuring that the controller is robust, the stability of the closed loop system is proved, by checking that the eigenvalues of $(A - BK)$ matrix are on the left half plane.

3.5 Proportional Integral control

In this case, the state of yaw rate is used to formulate the error $e(t)$ required by the PID theory. The error has the form

$$e(t) = \int_0^t r(\tau) - \dot{\psi}(\tau) \quad d\tau \tag{3.23}$$

It should be noted that in contrast with model based control techniques, only one state is chosen as control input, i.e. to be controlled. Thus, the PI controller does not a require a linear model to be designed. The next step would be to chose the gains K_p and K_I for properly formulating the proportional and integral terms. The gains are chosen according to the performance desired by the closed-loop system. For this case, the gains chosen for the non-linear closed loop system are the following

$$K_P = 0.01$$
$$K_I = 10$$

3.6 Linear Quadratic Integral control

For the design of the Linear Quadratic Integral control, the procedure is almost identical with the one of the Linear Quadratic Regulator. The only difference is that an error is augmented to the system, which is integrated and fed as input to the controller to achieve reference tracking. In this project, where the drifting of the vehicle outside of its lane has to be avoided, the state of yaw rate is chosen as the error that would be minimized.

Consequently, the additional state would have the form

$$z(t) = \int_0^t (r(\tau) - \dot{\psi}(\tau))d\tau \tag{3.24}$$

As mention in the Background section 2, the control input consists of two parts, and consequently two control gains K_x and K_I. The augmented state has to be taken into consideration while designing the weights for the cost functional. The dimensions should match and be according to the number of states of the controller plus the states added as integral states. Moreover, the integral states should be penalized to meet the performance expectations of the closed loop system and is done by using arbitrary gains, focusing on the yaw rate and its integral state.

The robustness of the controller is ensured by investigating the stability of the closed-loop system. The eigenvalues of the A_I matrix in equation (3.25) should be on the left half plane.

$$\dot{x} = \underbrace{\begin{bmatrix} A - BK_x & -BK_I \end{bmatrix}}_{A_I} \begin{bmatrix} x \\ z \end{bmatrix} \tag{3.25}$$

3.7 1-DoF $\mathcal{H}_\infty$ Controller

High uncertainty in the system, and the low natural frequency of an EPS centered steering system, motivate an $\mathcal{H}_\infty$ robust control approach. In this case, the signal response in the frequency domain needs to be analyzed and accounted for, which no conventional controller is able to perform. As for the uncertainty, both of the systems in question are subject to non-linearities triggered by parameter change. That is, velocity, cornering compliance, and tyre friction for the vehicle dynamics models, and mechanical friction for the steering system.

In contrast with the rest of the controllers, robust control requires a more complex tuning, by choosing dynamic weights for the inputs and the outputs of the system, as well as defining performance and measurement inputs/outputs.

3.7.1 Closed-loop system interconnection

First, the performance outputs of the system are defined for disturbance rejection. Disturbance rejection in this context means that the lateral forces applied do not affect the behavior of the vehicle, i.e. the vehicle is kept on track. To penalize the path deviation, the yaw rate $\dot{\psi}$ and the side slip angle β were chosen to be the performance outputs of the closed-loop system. Moreover, all the states of the nominal plant are considered to be measured outputs, thus inputs to the controller system $(K(t))$. As exogenous input to the system, the body force disturbance due to road bank angle is used. Moreover, the original inputs of the plant, the torques provided by the driver and the electric motor, are included as well. Consequently, the augmented system will have the disturbance, and the torque inputs as w, plus the control signals u_k provided by the controller, which in that case is one overlaid motor torque. At the same time, it contains 8 outputs, the measurement outputs of the system plus the performance outputs. It is thus an 8 by 4 system.

The signals of this system are

$$z = \begin{bmatrix} \beta \\ \dot{\psi} \end{bmatrix}, \ w = \begin{bmatrix} d \\ u \end{bmatrix}, \ u = \begin{bmatrix} T_h \\ T_m \end{bmatrix}, \ y = \begin{bmatrix} \theta_s \\ \dot{\theta}_s \\ x_r \\ \dot{x}_r \\ \beta \\ \dot{\psi} \end{bmatrix} \tag{3.26}$$

From the open loop partition equation (2.22), the same form is kept, but the control input notation u is changed to u_k and output v to the more general y, for better clarity with the other controllers.

The plant is then augmented with weights to get the frequency shape wanted. The augmented plant is a combination of the transfer function of the nominal plant and the weights chosen for the input and output parameters. Weights for the torque inputs W_u as well as the control input W_{uk} were chosen.

For representing the augmented plant in a sufficient way, the following transfer functions are derived by the nominal plant

- $P(z, w)$: The transfer function of the nominal Plant from the inputs of the plant to the nominated performance outputs side slip angle β and yaw rate $\dot{\psi}$.
- $P(z, u_k)$: The transfer function of the nominal Plant from the control signals to the nominated performance outputs side slip angle β and yaw rate $\dot{\psi}$.
- $P(y, w)$: The transfer function of the nominal Plant from the inputs of the plant to the nominated sensed outputs of the system.
- $P(y, u_k)$ The transfer function of the nominal Plant from the control signals to the nominated sensed output of the system.

The system interconnection can be seen in Fig 3.5. In the pure disturbance rejection case though, there is no reference, i.e. $r = 0$, thus it is not included. By rearranging into the general interconnection from Fig 2.12, i.e. following equation (2.22), the corresponding augmented plant P_{aug} becomes

$$\begin{bmatrix} z \\ y \end{bmatrix} = \underbrace{\begin{bmatrix} W_p P(z,w) W_w & W_p P(z,u_k) W_{uk} \\ P(y,w) W_w & P(y,u_k) W_{uk} \end{bmatrix}}_{P_{aug}} \begin{bmatrix} w \\ u_k \end{bmatrix} \tag{3.27}$$

where $W_w = diag(W_d, W_u)$.

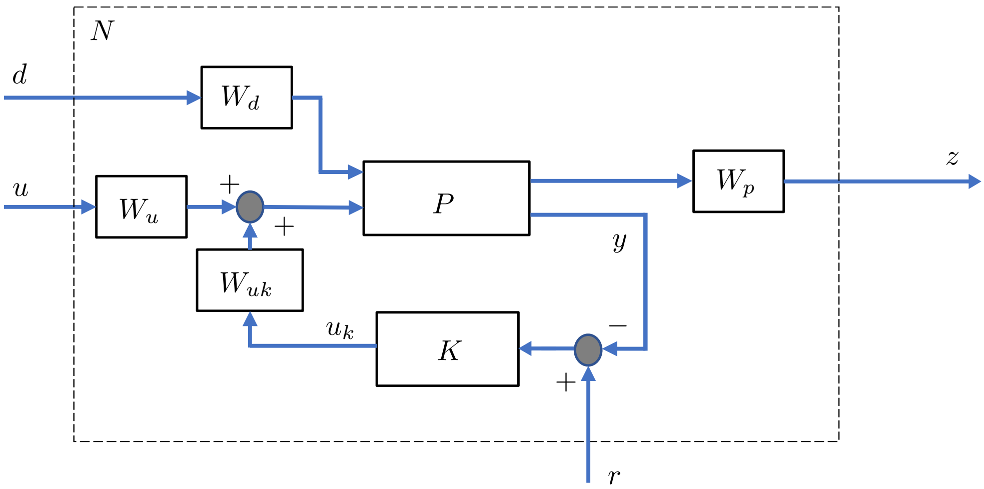

Figure 3.5: System Interconnection 1-DoF $\mathcal{H}_\infty$

3.7.2 Parametric Uncertainty

A system is robust when is able to compensate the differences between the system that the controller is used and the system that was designed. For defining these differences in the designed system, the parametric uncertainties are used. In this case, the parametric uncertainties included in the system are the cornering stiffness for the front and rear axis, the mass and the longitudinal velocity of the vehicle for the bicycle model, and the column spring and damping friction parameters for the steering system.

The reason for choosing the mass, moment of inertia, and speed of the vehicle is that these parameters are always changing. For instance, the total mass and moment of inertia changes depending on the number of passengers and luggage, while speed deviates as the car accelerates or decelerates. As for the cornering stiffness, it is a parameter that has a crucial role on the vehicle behavior and the translation of the lateral forces on the rack. Cornering stiffness can be affected by the type of tires or the road and driving conditions and its value differs for different scenarios. Finally, friction in the steering has already been discussed to be highly non-linear and uncertain. The column friction parameters influence the system the most and were chosen because of that.

For introducing the uncertainties in the Plant parameters, the *ureal*() function of the Robust Toolbox in Matlab was used [24]. The parameters were chosen to have the following deviation from their nominal value

- Vehicle Dynamics:
  - Front and Rear Cornering Stiffness (C_1, C_2): ± 30 %
  - Total Vehicle Mass (M_{tot}): $[-5, 10]$ %
  - Total Moment of Inertia (I_z): $[-5, 10]$ %
  - Vehicle Speed (V): ± 5 %
- Steering System:
  - Column Stiffness Coefficient (K_s): ± 50 %
  - Column Damping Coefficient (B_s): ± 50 %

Speed variation could be increased to include the whole approximation region of the bicycle model (from about 30 kph and above), however, the controller becomes too expensive. Results also showed substantial behavior even without this expansion. The system reaction to these uncertainties can be seen in Fig 3.6. Their effect are mainly in the low frequency region, which was to be expected as high frequencies are dampened by the system itself. The friction parameters $[K_s, B_s]$, move mostly the natural frequencies a bit, however, as their values remain within the same factor of ten, the effect is minimal, and are easily overbound in the filter design.

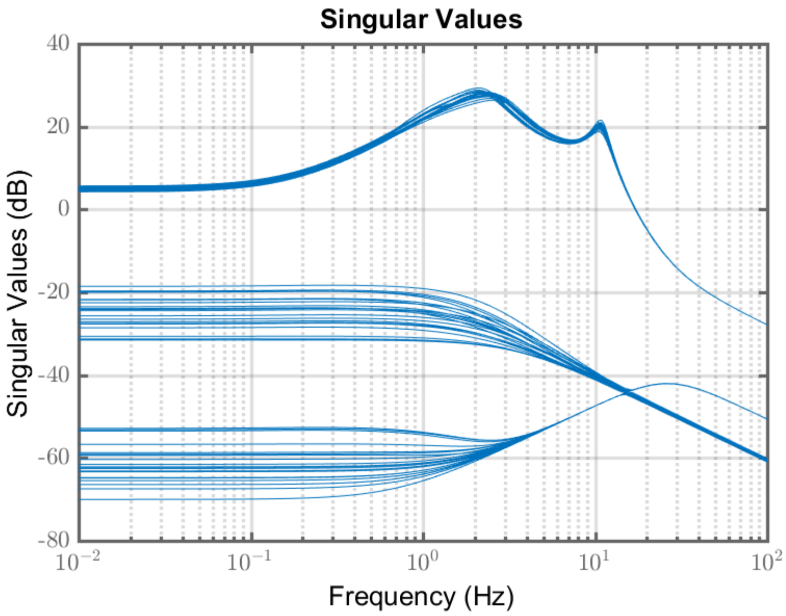

Figure 3.6: Singular Values of the enhanced with uncertainty Nominal Plant

3.7.3 Frequency Analysis of System Signals

To tune the controller properly, correct choice of the plant's weights is needed. The basic idea of the plant augmentation is to feed controller with knowledge of what to expect from the different signals. Based on data, a frequency analysis was conducted for all the signals considered relevant. Then, the weights were chosen to overbound the frequency response of these signals. For the controller's best response, weights for the driver and motor inputs, the control input, the disturbance, and the performance outputs were designed. In the next figures, the weight selection is described.

As test data including random banking is not easy to find, a test scenario was created in CarMaker. A road of 13 kilometers was built, which consists of turns as well as straight road segments, both with positive and negative lateral slopes that vary from 1 to 7 %. The virtual driver was chosen to follow the lane, not drifting away from its path no matter the level of disturbance.

Afterwards, the signal frequency analysis was made, by conducting a fast Fourier transform (FFT) in Matlab. Based on these frequency responses, the dynamic tuning of the robust controller was made, by choosing the weights accordingly. In Figure 3.7, at the left part 3.7a, the road disturbance due to banking can be seen, while at the right part 3.7b the yaw rate and slip angle signals' response are depicted. With dashed lines the corresponding weights are ploted. The performance weight is approximated with a low pass filter, which therefore boosts the control behavior at low frequencies as well. As for the inputs to the plant, the filtering is depicted in Fig 3.8. This filtering has not been as easy as the other parts mainly because the controller adding torque to the motor, triggering mainly the second natural frequency of the system around 10 Hz. In order for the controller to be more careful, both of the plant inputs' filters present a bump at that point. Finally, a dynamic weight for the control signal was selected as presented in Figure 3.8c. This one had to be made in cases where the controller was active, to get the reeuired data. The filtering of the control feedback signal provides is contributing to the compensation of oscillations and jittering behavior while at the same time ensures that the torque boost, does not cross the predefined limits and the EPS system would be able to deliver it.

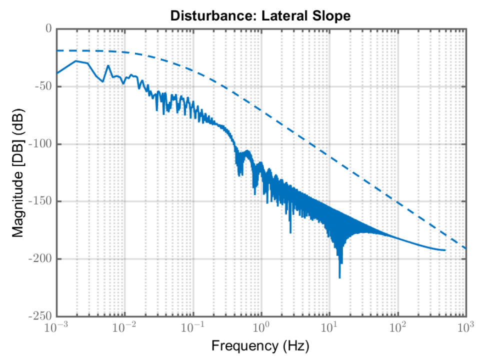

(a) Disturbance FFT

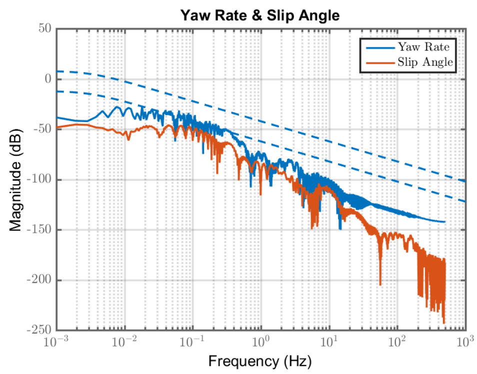

(b) Performance FFT

Figure 3.7: Frequency analysis of the performance and disturbance response

Finally, it is worth knowing that the weight of the motor and controller had to be increased slightly for the reference case. That can be explained as more torque needs to be added to both follow the reference and reject the disturbances.

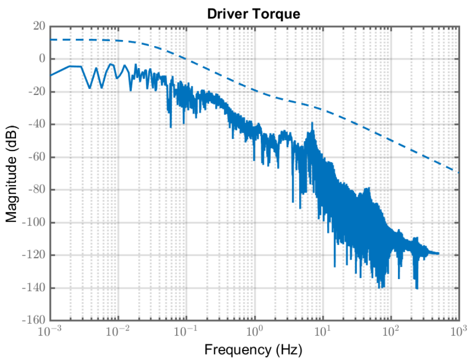

(a) Driver's Torque FFT

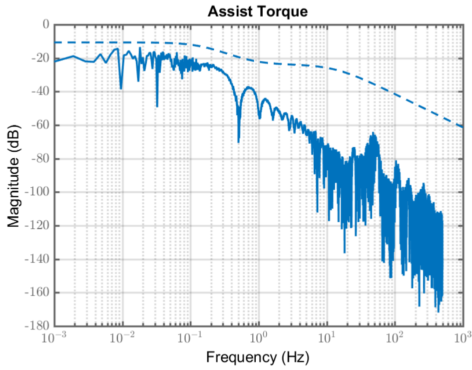

(b) Electric Motor Torque FFT

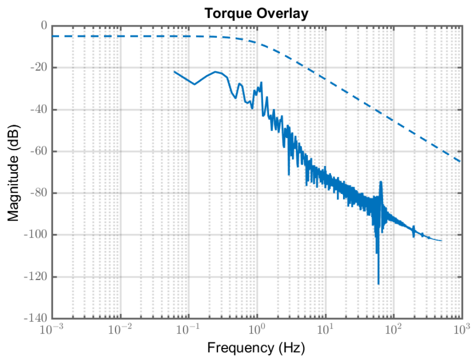

(c) Control Signal FFT

Figure 3.8: Frequency analysis of the input response

3.8 2-DoF $\mathcal{H}_\infty$ Controller

The system is expanded to 2-DoF, to include reference tracking in the controller's description, for better results. The addition of the reference directly in the controller changes the system interconnection slightly. The new system can be seen in Fig 3.9, while its equation reads

$$\begin{bmatrix} z \\ r \\ y \end{bmatrix} = \underbrace{\begin{bmatrix} W_p P(z,w) W_w & W_{p2}(W_0 - T_{ref}) & W_p P(z,u_k) W_{uk} \\ 0 & I & 0 \\ P(y,w) W_w & 0 & P(y,u_k) W_{uk} \end{bmatrix}}_{P_{aug,r}} \begin{bmatrix} w \\ r \\ u_k \end{bmatrix} \tag{3.28}$$

where W_0 is a selector of the yaw rate.

Before, there was only the error signal $y - r$ fed to the controller, whereas now a new r signal enters the system. The reference signal can either be taken from the system's input u and translated through a T_{ref} transfer function into yaw rate or enter as yaw rate directly though a look-up table. The first approach is unfortunately only limited to small values of driver torque, as the 3$^{\text{rd}}$ order boost curve of the motor escapes the linearization region.

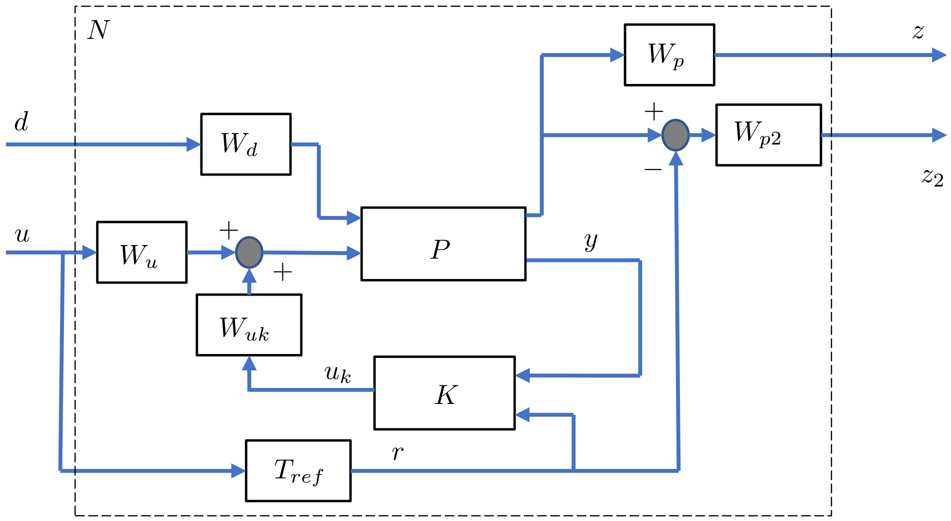

Figure 3.9: System Interconnection 2-DoF $\mathcal{H}_\infty$

For better reference shaping a filter W_r can be added. A usual form found in literature [25] expresses the input to output as a 1st order lag, in that case

$$T_h = \frac{\rho}{t_p s + 1} \tag{3.29}$$

where ρ denotes the gain, which can be used to correct steady state differences as in Fig 2.15, while t_p is the driver's delay time constant. Usual driver reaction times are at about $t_p = 0.15$, and for a $\rho = 1$, the reference filter becomes

$$W_r = \frac{1}{0.15s + 1} \tag{3.30}$$

3.9 Long Term Compensation

Long term asymmetry effects of a vehicle are unknown and depend on the current situation both of the vehicle itself and its surroundings. They cause the vehicle to drift away from a straight line, which the driver has to correct. M. Kubota et al. [26] studied those phenomena from a statistics point of view, and proved that the driver's torque input to compensate for them, when driving straight, is normally distributed. That simplifies much an estimation procedure, as the mean and variance can be easily computed. After estimating an average driver torque by gathering data, this value can be translated into the motor and applied as a constant overlay torque. That is, $\hat{\mu} = T_{h0}$ in eq. (2.42), with T_{h0} being the average driver torque at straight-line driving. The driver to motor torque is translated from the steering wheel to the rack through the pinion, and to the motor through the motor's transmission, resulting in

$$H_{T_h \to T_m} = \frac{1}{g_m} \tag{3.31}$$

(see (3.12)-(3.19) for details). The value of T_{h0} can be taken directly from the torque sensor.

The driver's torque at straight-line driving is measured and data are gathered at intervals. Straight-line driving is assumed to be at zero yaw rate. In practice below a yaw rate value the vehicle is assumed to be driving straight. That was chosen to be

$$| \dot{\psi} | \leq 3 \cdot 10^{-3} \tag{3.32}$$

based on this paper.

Based on equation (2.44) a first sample size is estimated. For a confidence interval α of about 4.5 % $Z_{1-\frac{\alpha}{2}} \approx 2$, acceptable error $d = 10$ %, and variance $\sigma^2 = 1$ Nm, gives a sample size $n \geq 400$, which comes in fact true with the results on [26]. The value for the variance was taken by that paper, based on their test results. This value corresponds to the fluctuation around the mean, which comes mainly because of friction. It is a big value of variance, that is why the sample size becomes quite big as well.

To construct a proper random sample, systematic sampling was used. That is, as the simulation runs in continuous time, a large sampling time was used to get the required data. A note here is that to be sure about sensor bias, this sampling frame should be changed for every sample being taken. Ideally with the equiprobability method. For the simulation different sampling frames were tested, but no bias was found as it was expected from a computer based simulation.

4
Results

In the current section, a closer look is given to the validation of the control strategy in both the linear and the non-linear model. The procedure followed is depicted in Figure 4.1. The different control strategies were implemented and tuned in the linear control model and then applied to the more complex one, in order to derive the proper results. Moreover, a comparison between the strategies has been conducted, in order to get a closer look at the controller's behavior, as well as to derive the proper conclusions regarding their performance in a high fidelity system. In order to test the performance, a driving scenario

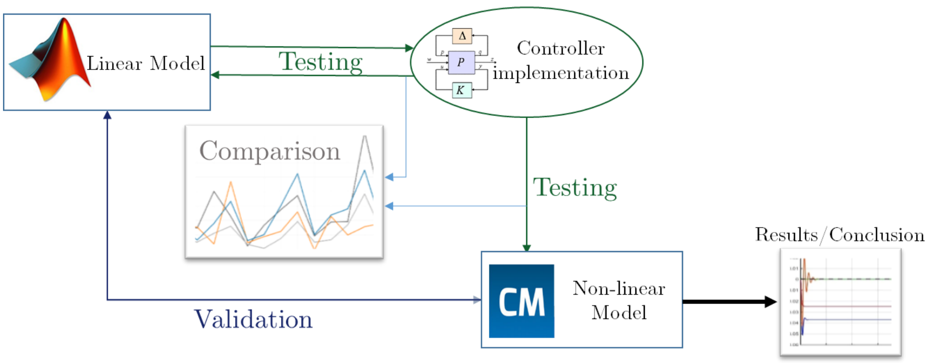

Figure 4.1: Validation graph

should be implemented. The driving scenario is a simulation environment, in which the disturbance and the driver behaviour can be predefined, as well as different parameters regarding the road, such as inclination and slope profile. In addition, to verify that the disturbance is actually rejected and to study the vehicle behaviour, an approximation of the vehicle trajectory is used. The approximation function (see Appendix (A.1)) uses the data acquired by the yaw angle, the yaw rate and the slip angle β to derive the path of the vehicle in XY plane. It should be noted that in case of no disturbance, the vehicle's path should be at zero.

First, a comparison of the linear model to CarMaker in open loop is presented. It is good to know that CarMaker uses a complex model for the steering system [23], including the non-linear friction expressions, based on [22]. Then, the performance of the controllers are presented, both in the linear and CarMaker closed loops.

4.1 Open Loop Comparison

The linear model was added to the Simulink-CarMaker environment and comparisons for different scenarios were made. Some parameters had to be tuned to give a closer connection. Those were mainly the spring and damping parameters for the column and rack, as friction was added to those terms. As the rack was enhanced from the motor's and wheels' influence, very small adjustments had to be made. In other words, the rack's parameters $[M_r, K_r, B_r]$ have been increased that much that the frictions had a minimal effect. On the column though, the magnitude has been much larger, resulting in big adjustments of the values of $[K_s, B_s]$, where the friction was added. This was done in such way

$$K_s' = K_s + K_{s,f} \tag{4.1}$$
$$B_s' = B_s + B_{s,f} \tag{4.2}$$

with f the parameters due to friction are denoted. In Figures 4.2-4.3, two tests are presented: a step input and a sinus sweep. For the step steer, the driver is putting 3 Nm torque. As for the sinus sweep, 5 different sinusoidal inputs are given, with their amplitudes ranging from 1.5 Nm to 3.5 Nm, and their time periods from 1 to 5 s.

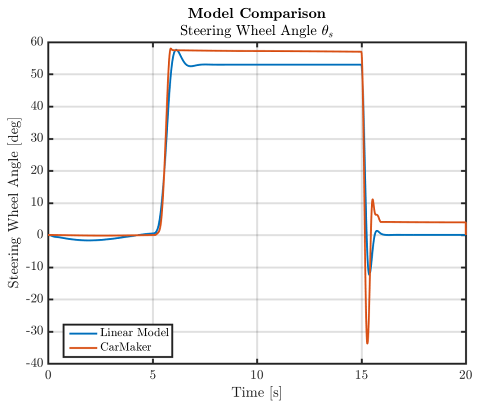

(a) SWA

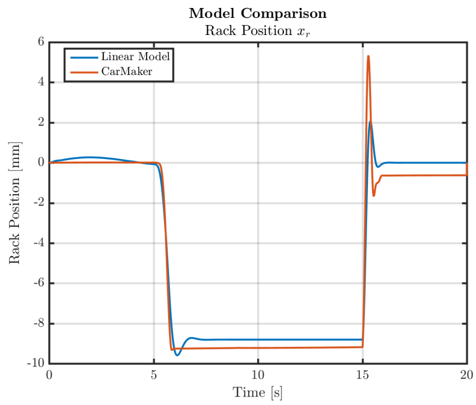

(b) Rack Position

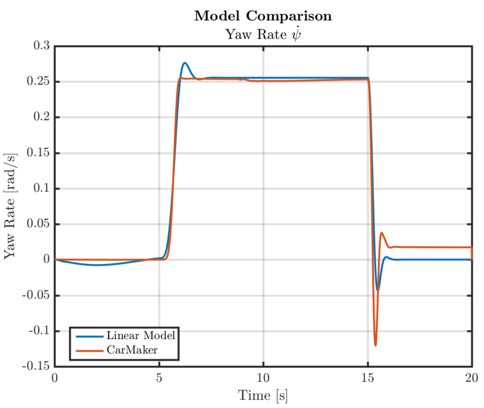

(c) Yaw Rate

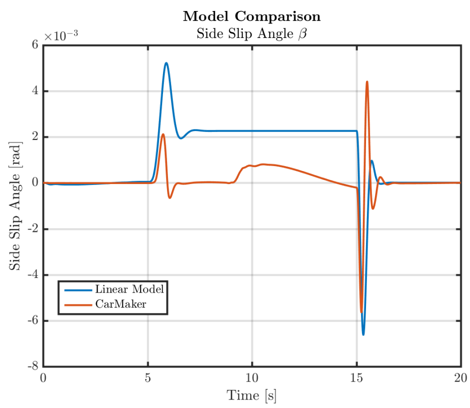

(d) Side Slip Angle

Figure 4.2: Open Loop - Model Comparison: Step Steer; $T_h = 3$ [Nm]

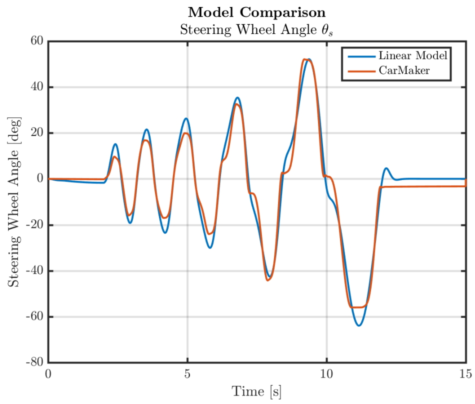

(a) SWA

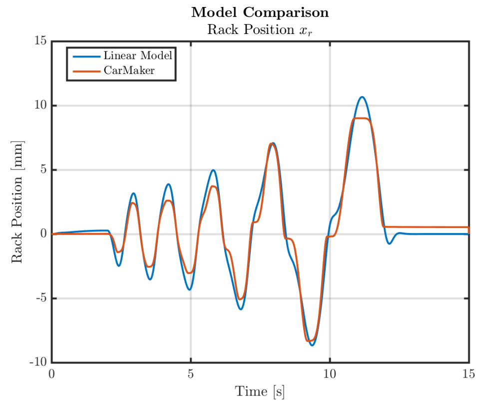

(b) Rack Position

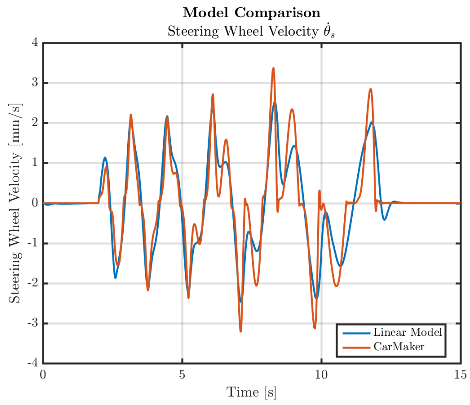

(c) Steering Wheel Velocity

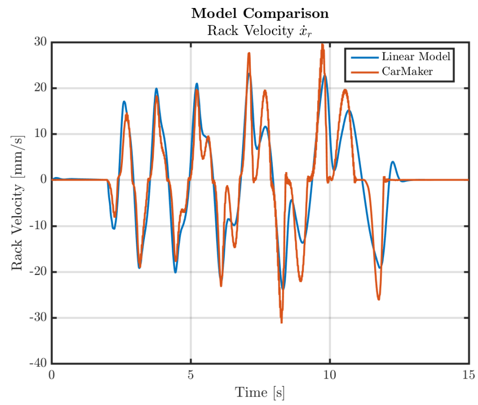

(d) Rack Velocity

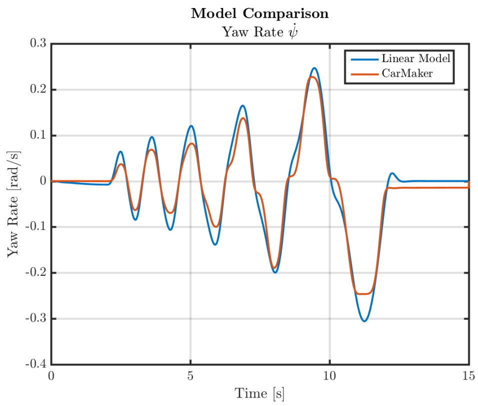

(e) Yaw Rate

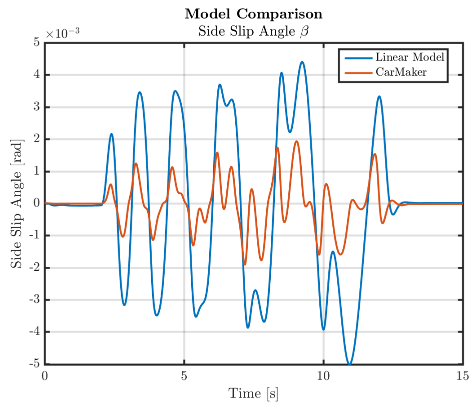

(f) Side Slip Angle

Figure 4.3: Open Loop - Model Comparison: Sinus Sweep; $T_h = 1.5 - 3.5$ [Nm], $T = 1 - 5$ [s]

It can be seen that the 2 models are quite close, for all the states but the side slip angle. The difference in magnitude of β is about 3 times in the dynamic case and many more in the step steer case. The dynamic behavior is similar though, despite the difference in magnitude. This is a known issue with the side slip angle, and even nowadays efforts for its correct estimation are made.

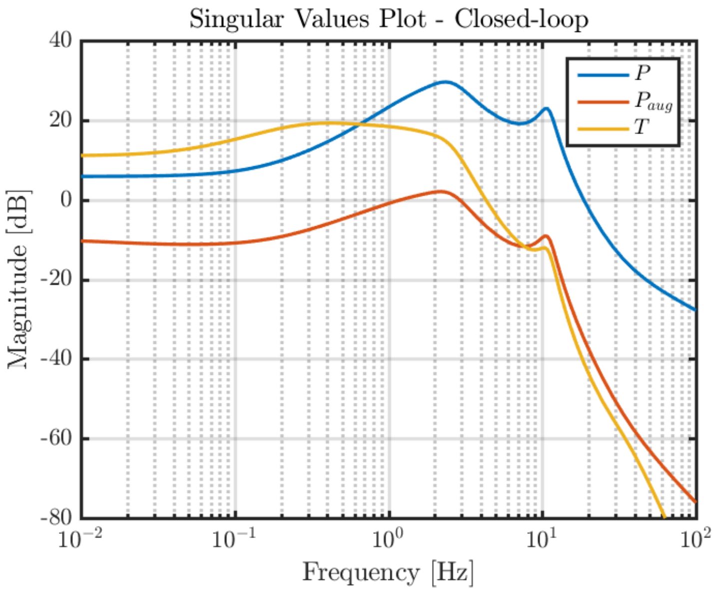

Figure 4.4: Closed-loop Plant Singular Values Comparison

4.2 Robust Control: Closed-loop Sensitivity

In Fig 4.4, the plant's frequency response is compared. P denotes the nominal plant, P_{aug} denotes the augmented, and T denotes the complementary sensitivity, which can be seen as the closed-loop transfer function. Compared to the nominal, the augmented plant is scaled down. This happens because of the weight choice presented in section 3.7.3. The majority of the weights are beneath the zero decibel line, resulting in magnitudes below one. In other words, the non-linear model's response to the same input is lower in the area of investigation. However, it can be seen that the closed-loop transfer function is scaled up. That is expected, as the controller adds extra torque to the motor. The controller though, targets only the frequency area indicated by the performance filters. More specifically, for about 0.2 Hz and below the behavior is enhanced, then, the area until the first peak at 2.5 Hz is flattened, and afterwards it is dampened. This shows the power of the robust control, which is able to maintain stability, while keeping the performance high in the wanted frequency areas.

4.3 Closed Loop Comparison: Disturbance Rejection

Four different controllers have been investigated. A Proportional Integral (PI) controller, a Linear Quadratic Regulator (LQR) controller, a Linear Quadratic Integral (LQI) controller and a 1 Degree of Freedom Robust (1 DoF $\mathcal{H}_\infty$) controller. For all the cases, the controllers provide the extra torque boost on the electric motor input, as an additional term.

The controller behavior was evaluated first in the linear model, and afterwards in the complex, nonlinear environment of CarMaker. The tuning of the model-based controllers was conducted first on the linear model and then applied on the non-linear. The only controller that required additional tuning was the PI controller. The reason is that PI provides local optimization, only at the state that is controlled and does not take into consideration the rest of the system's states. Thus, a linear model is not required for its tuning, however, it has to adapt on each model's behavior to perform accordingly.

It should be noted that both the linear and non linear models have the same disturbance and driver's torque Th. Moreover, the driver is not providing any torque to the vehicle, meaning that this is a "hands off" the steering wheel situation.

4.3.1 Test scenario 1

For this scenario, a 500 meter straight road has been chosen, with a step in the lateral slope of 7% (4 degrees). The disturbance has the form as depicted in Figure 4.5 and reaches its steady state slightly after 12 seconds. Moreover, the width of each lane is 5 meters and the total width of the road is 12 meters. The width of the car, a Volvo XC90 which is modelled in this case is about 2 meters, including the mirrors.

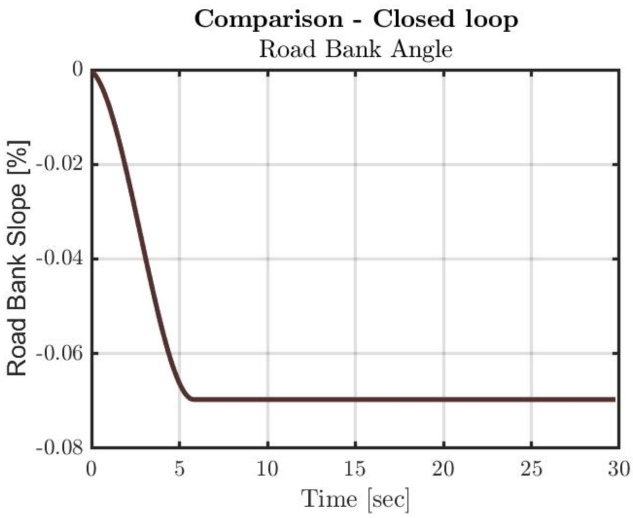

Figure 4.5: Road Bank Slope: Test Scenario 1

4.3.1.1 Linear Model

In this section, the behavior of the 2-mass linear model in the same simulation test as the linear model will be investigated, while it is connected with different types of controllers that provide a feedback to the system. Hence, a closed-loop system is formulated, with the inputs of the system affected by the controller output.

As depicted in Figure 4.6a, the yaw rate has been decreased to zero compared to the open loop case. The $\mathcal{H}_\infty$ controller has promising results, as it manages to decrease effectively the yaw rate $\dot{\psi}$ with minimal oscillatory behavior. The Linear Quadratic controllers have similar performance, although LQI is more effective in decreasing yaw rate due to the fact that an integrated state has been chosen. The PI controller, which optimizes locally only the yaw rate state, manages to minimize yaw rate in an effective level as well, although there is some overshoot in the beginning.

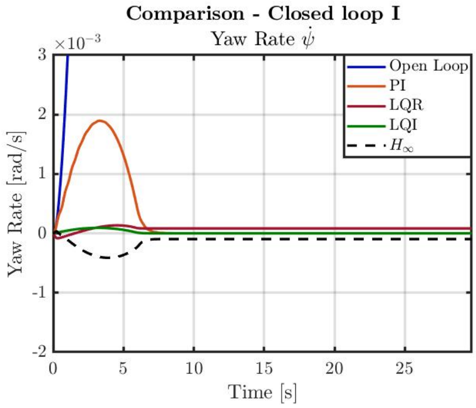

(a) Yaw Rate

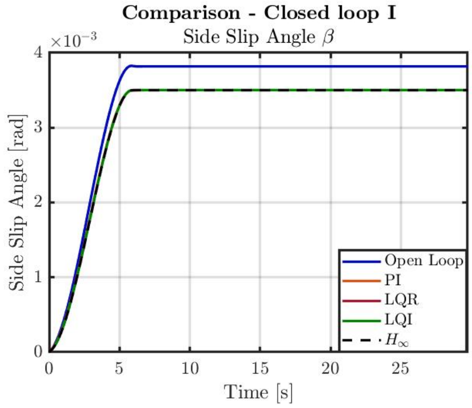

(b) Slip angle β

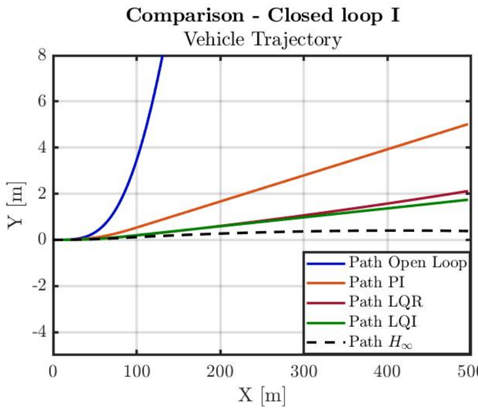

(c) Vehicle Trajectory

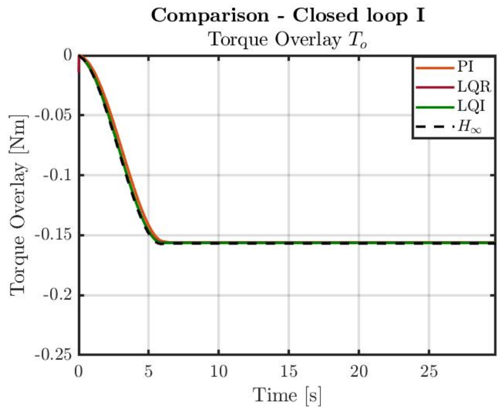

(d) Torque overlay T_o

Figure 4.6: Linear closed-loop model parameters for Test Scenario 1

As for the side slip angle, the results are shown in Figure 4.6b. The value reached is quite close to the open loop is reached. This is an indication that the side slip angle cannot be minimized more. Practically, the vehicle slips and in order to reduce the slip angle, larger values of steering wheel angle would be required, which would eventually turn the vehicle the other way around, making yaw rate negative. That can be explained by looking at the equations of the bicycle model (3.8). For the case of zero disturbance, β and $\dot{\psi}$ are zero for $\delta = 0$. With non zero disturbance though, that is not the case, as β and $\dot{\psi}$ cannot be zero at the same time.

As shown in Figure 4.6c, all of the controllers manage to reduce the drift of the vehicle, comparing to the open loop case. However, the $\mathcal{H}_\infty$ and LQI controller have the best results, followed by the LQR controller. In addition to that, the open loop behavior matches the expected of section 2.1, also showed schematically on Fig 2.1.

Moving to Figure 4.6d, an insight on the torque overlay provided by the e-motor can be seen. As mentioned in previously, there is a threshold limit in the extra boost that can be provided by the electric motor. In this case, all the controllers are below this limit. Although all controllers reach more or less the same steady state value, the $\mathcal{H}_\infty$ controller, provides a bit faster response resulting in the best vehicle behavior in terms of lane keeping.

As a reminder, for the robust controller both of those states were chosen as performance outputs, while for the rest of the controllers, only the yaw rate was penalized to achieve the desirable performance. The main reason for this choice had been the behavior of the controllers when β was included as a performance state, as only the robust controller gained advantage of using it. The tuning for the robust controller was much easier and the response stabler, when including β. This could be explained as dangerous dynamics (that would increase slip) are avoided. The advantage though, cannot be reflected in this particular scenario. It will be more clear in the reference tracking results.

4.3.1.2 Non-Linear Model

The controllers designed in the linear model, are now tested in CarMaker. Regarding the yaw rate, the behavior of the controllers is similar as in the linear model simulation, since all of them try to get the yaw rate to zero. This result is shown in Figure 4.7a. The oscillations in the yaw rate on this case, were not present in the linear model. They appear mainly due to non-linearities in the system, like for instance differences in the friction forces between the two models.

For the slip angle though, in Figure 4.7b, all of the controllers reach the same value, the one of the open loop as in the linear case. A value of the same magnitude is reached as well.

In Figure 4.7c an approximation of the trajectory followed by the vehicle can be shown, as well as the extra torque provided by the EPS system in Figure 4.7d. The results are similar as well, with the difference that in this case the effect of the disturbance in the system is larger and none of the controllers have the ideal performance of the linear model.

The torque overlay (T_o) term is depicted in Figure 4.7d. The pre-defined threshold is not violated for all control cases, although the extra boost is twice in magnitude compared to the linear closed-loop simulation.

On table 4.1 a comparison of the steady state values between the variables that affect the path of the vehicle is presented. As reflected by the Figures as well, the final values of the signals are very close. The only difference is noticed in the case of the torque boost, where in the non-linear model has almost twice the size. In addition, by using a controller with an integral part, the yaw rate is basically zero, achieving values much smaller comparing to the rest of the controllers.

4.3.2 Test scenario 2

For this scenario, a 1000 meters straight road has be chosen, with a road bank angle that is changing non-periodically. The magnitude of the slope is varying from -7 % to 7 %. The disturbance has the form depicted in Figure 4.8. Moreover, the same parameterization, regarding road width and vehicle model, as is Test Scenario 1 is used.

First, the behaviour of the linear closed-loop model will be presented focusing on the yaw rate and slip angle of the vehicle, and then by using the same disturbance and torque

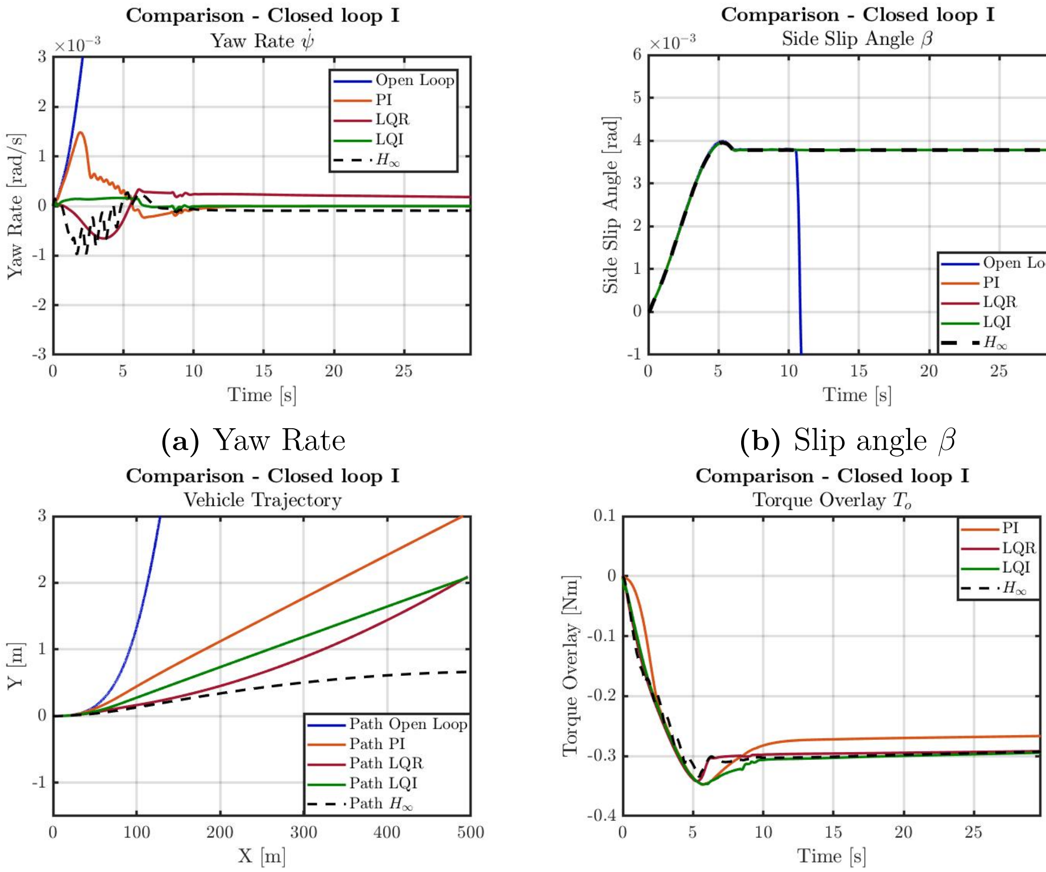

(a) Yaw Rate **(b)** Slip angle β

(c) Vehicle Trajectory **(d)** Torque Overlay T_o

Figure 4.7: Parameters of the closed loop non linear model for Test Scenario 1

	Parameter	**Linear Model**	**Non-Linear Model**
$\mathcal{H}_\infty$	$\dot{\psi}$ [rad/s]	-9.6×10^{-5}	-9.3×10^{-5}
	θ_s [rad]	-2.9×10^{-2}	-3.3×10^{-2}
	T_o [Nm]	-0.157	-0.293
LQI	$\dot{\psi}$ [rad/s]	2.6×10^{-17}	-8.4×10^{-8}
	θ_s [rad]	-2.8×10^{-2}	-3.3×10^{-2}
	T_o [Nm]	-0.156	-0.295
LQR	$\dot{\psi}$ [rad/s]	8.3×10^{-5}	0.8×10^{-5}
	θ_s [rad]	-2.8×10^{-2}	-3.27×10^{-2}
	T_o [Nm]	-0.156	-0.292
PI	$\dot{\psi}$ [rad/s]	2.3×10^{-17}	-3.4×10^{-6}
	θ_s [rad]	-2.8×10^{-2}	-3.3×10^{-2}
	T_o [Nm]	-0.156	-0.266

Table 4.1: Closed-loop model comparison

provided by the driver, the performance of the vehicle will be simulated in the non-linear model. Moreover, an approximation of its trajectory is depicted as well as a plot of the control input, i.e the Torque overlay provided by the EPS.

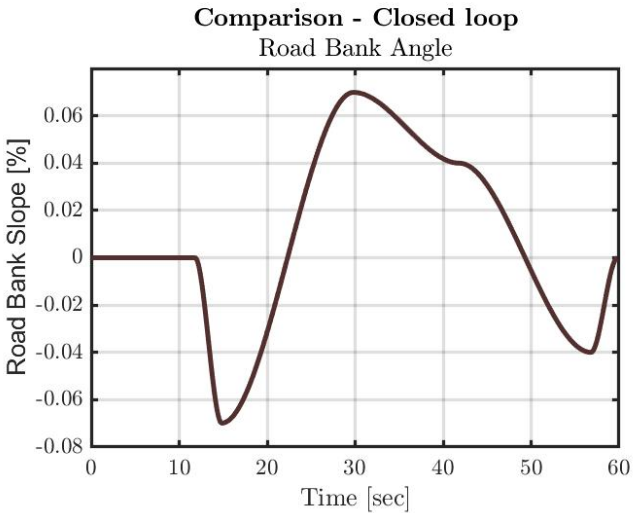

Figure 4.8: Road Bank Slope: Test Scenario 2

4.3.2.1 Linear Model

As depicted in Figure 4.9, the yaw rate has been decreased significantly compared to the open loop case. The $\mathcal{H}_\infty$ controller has the most promising results, together with the Linear Quadratic Integrator. The performance of the PI and LQR controllers might not be the same, but manage to keep yaw rate in low values during the simulation.

The control strategies manage to decrease slip angle β as well, compared to the open loop case. The slip angle behaves the same for all control cases, for the same reasons explained in the section before.

For the case of the linear model, all the controllers manage to reduce the drift of the vehicle, as shown in Figure 4.9c comparing to the open loop case. However, the $\mathcal{H}_\infty$ and LQI controllers have better performance than the rest.

Finally, the extra Torque term (T_o) is between the acceptable limits and the torque request is more or less the same for all the control methods.

4.3.2.2 Non-Linear Model

In Figure 4.10, the yaw rate $\dot{\psi}$ and side slip angle β are presented. Some oscillations may arise, in the $\mathcal{H}_\infty$ and PI cases, due to the nature of the disturbance. These oscillations though are dampened by the system, ending in even smaller ones in the steering wheel, which should not be noticeable by the driver. The LQI controller has a smoother performance, as shown in Figure 4.10a.

Regarding the slip angle, all the controllers end up at the same value, the slip angle of the open loop system. In Figure 4.10b, the open loop blue line is cut off suddenly, because the vehicle model gets out of the road after 17 seconds.

Similarly with the previous sections, the vehicle trajectory and the torque boost provided

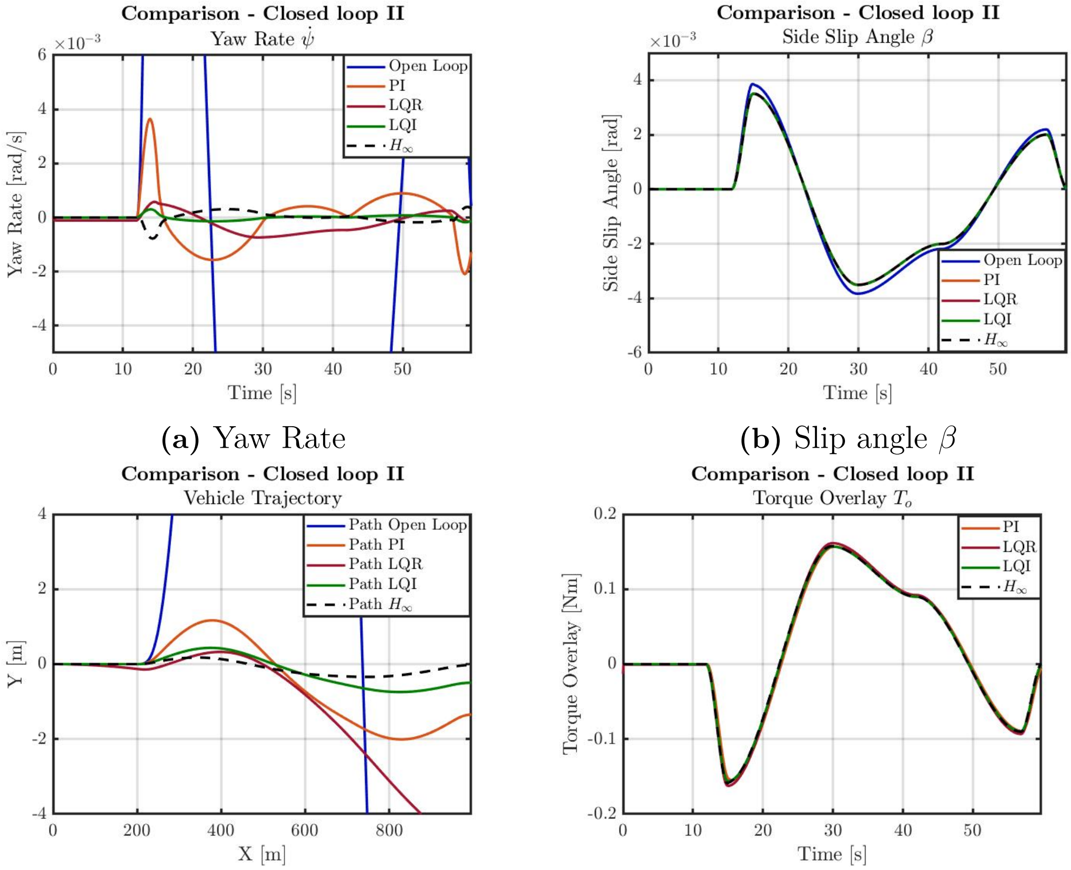

(a) Yaw Rate

(b) Slip angle β

(c) Vehicle Trajectory

(d) Torque overlay T_o

Figure 4.9: Parameters of closed loop linear model for Test Scenario 2

by the EPS system are showcased in Figures 4.10c and 4.10d. In this test scenario, the vehicle trajectory is the best for the $\mathcal{H}_\infty$ case, than for the rest of the closed-loop systems. The drift of the vehicle is close to 1 meter, with a lower overshoot.

4.4 Velocity adaptation

In this section, the performance of the controllers in different velocities will be investigated. As mentioned in Methods, the $\mathcal{H}_\infty$ controller can be designed by taking into consideration that the value of the velocity is not stable. It can be introduced as a parametric uncertainty. However, this is not the case for the model-based controller LQI, as well as the PI controller. In the case of the LQI controller, it was designed, tuned and tested with taking into consideration that the vehicle's speed is a stable parameter, in 60 kilometers per hour. As for PI, a model is not required for its design, since it only consists of two terms that manipulate an error signal $e(t)$ of the yaw rate.

The performance of the controllers in this case was tested in the same simulation environment as Test Scenario 1. The road parameterization is the same and the disturbance is introduced as a step function that reaches its steady state at 5 seconds. However, the

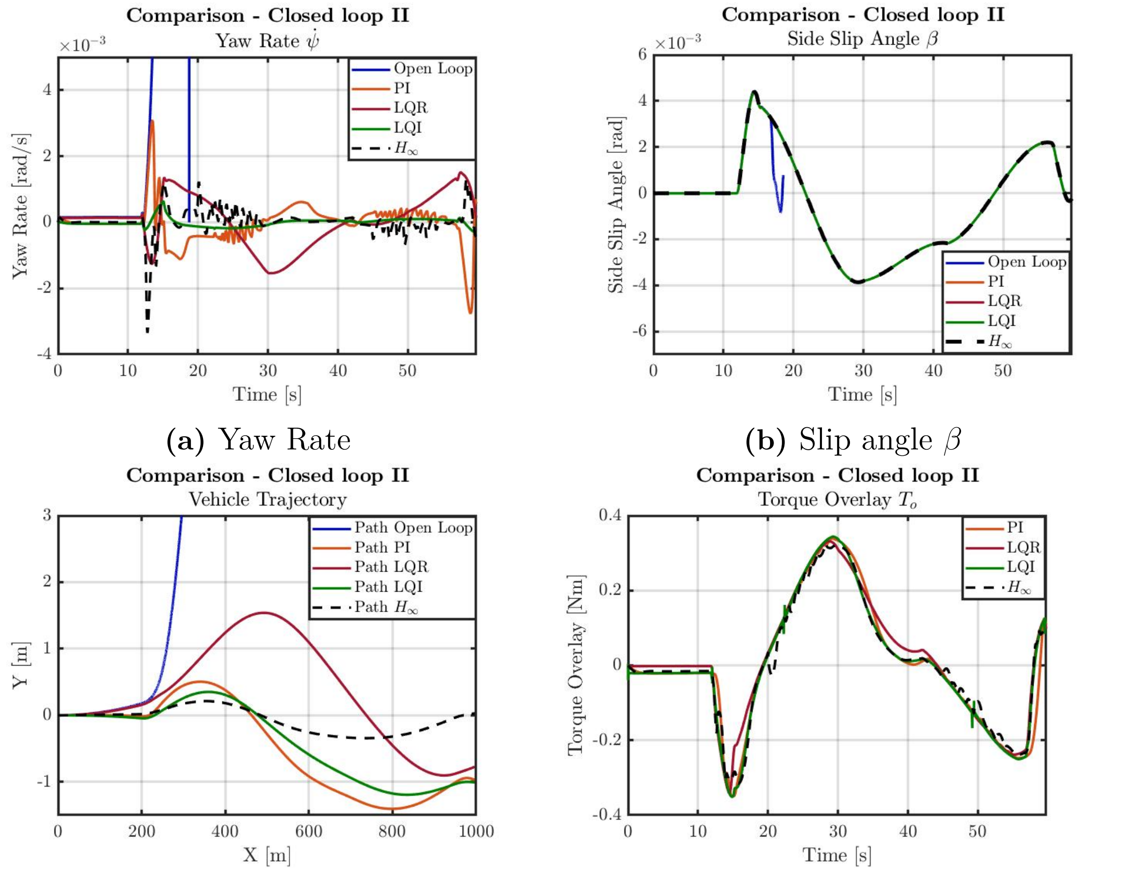

(a) Yaw Rate **(b)** Slip angle β

(c) Vehicle Trajectory **(d)** Torque Overlay T_o

Figure 4.10: Parameters of the closed loop, non-linear model for Test Scenario 2

vehicle is not always moving with a steady speed, but it is accelerating up to the following values:

- 45 km/h
- 60 km/h
- 90 km/h

Moreover, the non-linear closed-loop model is used, since the goal is to obtain results that are as close as possible to reality. Regarding the parameters tested in this case, yaw rate, estimated trajectory and torque overlay will be presented.

In Figure 4.11b, it can be seen that the LQI control strategy has almost the same response for the yaw rate, no matter the longitudinal velocity of the vehicle. This can be explained, due to the integration effect of the augmented state. In Table 4.1 for instance, the values of the yaw rate are much closer to zero, compared to the other model-based controllers. As for the $\mathcal{H}_\infty$ closed-loop, the responses are close, with a small variation depending on the increase or decrease of the velocity, something that is not the case with PI, since yaw rate is having large oscillations in higher speeds, no matter the integration. This should be expected, since the variables that define the behaviour of the vehicle are not taken into consideration during the tuning of the controller.

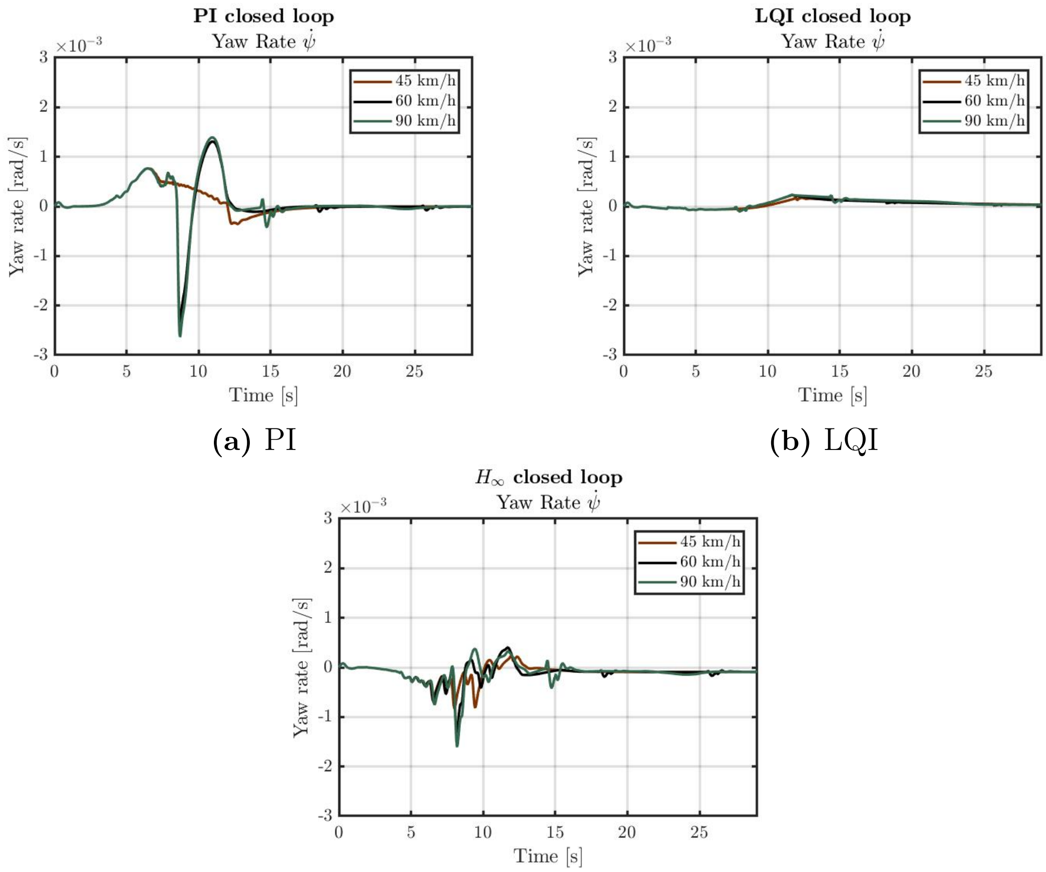

(a) PI

(b) LQI

(c) $\mathcal{H}_\infty$

Figure 4.11: Yaw rate response in different closed-loop cases for different velocities

In Figure 4.12, the extra boost provided by the Electric Motor in different velocities is presented. For all cases, the extra torque boost ends up in the same steady state region, between $[-0.2, -0.3]$ Nm. It is notable that for 45 km/h, LQI and $\mathcal{H}_\infty$ cases require a bigger boost than in 60 or 90 km/h. The reason for that is the nature of the nonlinear model, since at lower longitudinal velocity, more torque is required to turn the vehicle. On the other hand, this phenomenon is not present in the PI case due to the fact that PI design is not based on a model. Hence, the effects of the phenomenon is only reflected on the yaw rate.

Finally, the estimation of the trajectory of the vehicle for the three different cases is presented in Figure 4.13. For the LQI closed-loop system, the trajectory in all cases is exactly the same, showcasing good robustness in terms of velocity variation. However, in the $\mathcal{H}_\infty$ case, the the drift is less when comparing to the rest of the cases. For this case, as the speed increases, the drift increases, which can be explained due to the decreased response time needed. In the PI case, the drifting phenomenon is decreasing as the longitudinal velocity increases. It should be noted that for this scenario the vehicle covered the same distance in meters, but in different time, due to the difference in the vehicle's speed.

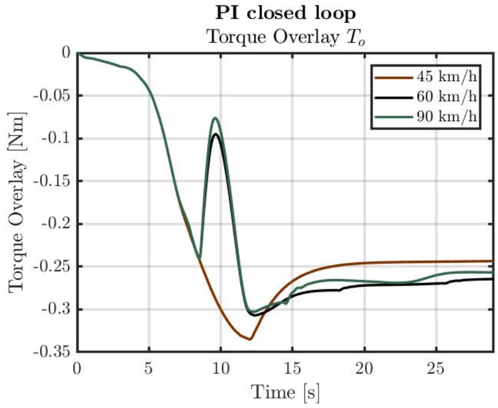

(a) PI

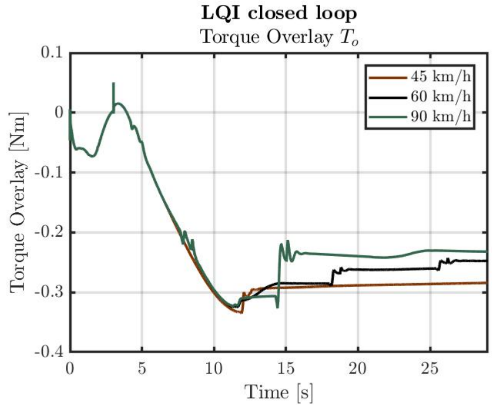

(b) LQI

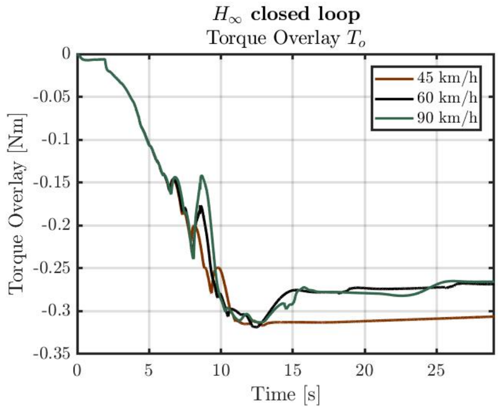

(c) $\mathcal{H}_\infty$

Figure 4.12: Torque overlay response in different closed-loop cases for different velocities

4.5 Additional Controllers

The control strategies implemented so far for mitigation of the disturbance consist of a typical PI controller, the Linear Quadratic Regulator and its integral form, and finally a model-based, 1 Degree of Freedom $\mathcal{H}_\infty$ controller, that requires dynamic tuning and is frequency dependent. Except for the PI controller, the rest of them require a linear model for their design and tuning, in order to provide state feedback. The input to the control gain or LTI system K is the states of the linear model $\begin{bmatrix}\theta_s & \dot{\theta}_s & x_r & \dot{x}_r & \beta & \dot{\psi}\end{bmatrix}'$.

In the case of the $\mathcal{H}_\infty$ controller, the performance outputs, the states that are minimized, are the yaw rate as well as the vehicle's side slip angle $\begin{bmatrix}\dot{\psi} & \beta\end{bmatrix}'$. One of the reasons that β is used as a performance output, except its importance in the lane keeping of the vehicle, is the difference in magnitude between the linear and the non-linear model. For the open loop, Figure 4.2d for instance, the dynamic performance between the models is similar but the magnitude is not.

The reduction of the states could be beneficial for the real-time implementation of the control strategy. In the nonlinear model, the simulation environment includes virtual

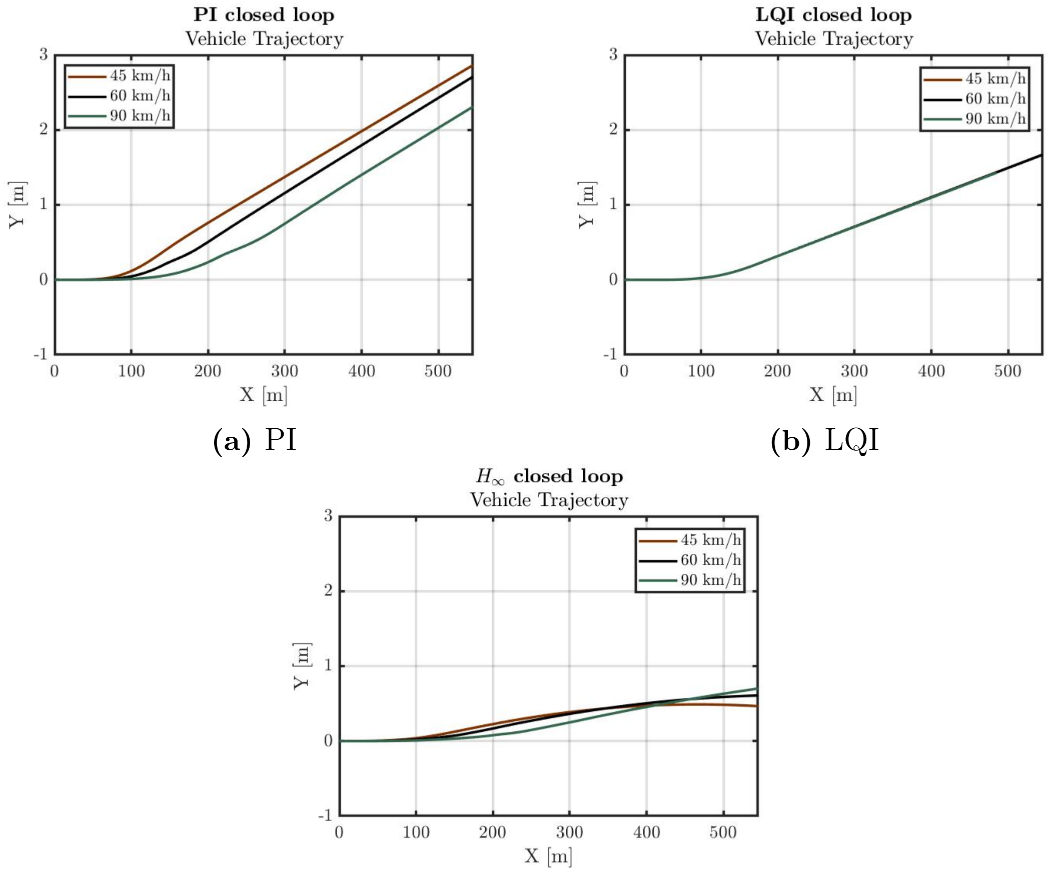

(a) PI **(b)** LQI

(c) $\mathcal{H}_\infty$

Figure 4.13: Trajectory in different closed-loop cases for different velocities

sensors, providing measurements based on the simulation. However, in most real life applications, the sensors can provide misleading results due to noise or misalignments. For the side slip angle, expensive optical sensors or other advancement measurement units are needed, which are not mounted in normal vehicles. Moreover, efforts have been made to estimate. Its estimation issues come from the lateral speed (see eq. (3.3)), which can be taken after lateral acceleration measurement and integration. This integration results in high error. Even today, research is ongoing to find a good estimation technique.

In order to provide a more robust approach for a real-time implementation of the control strategy, a 1 Degree of Freedom $\mathcal{H}_\infty$ controller with a reduced number of measurement and performance states is designed. The measured states, the inputs in the controller, have been chosen to be: the steering wheel angle θ_s, the rack displacement x_r and the yaw rate $\dot{\psi}$, which is also considered as the only performance output, as shown below. The differentiation to get the velocities of the rack and column could be added, however, in simulations they gave minor benefits.

$$z = \begin{bmatrix} \dot{\psi} \end{bmatrix} \tag{4.3}$$

$$y = \begin{bmatrix} \theta_s \\ x_r \\ \dot{\psi} \end{bmatrix} \tag{4.4}$$

Similar as before, the performance of the closed-loop systems will be compared in a scenario where the disturbance has the form of a step function. Then, the same comparison will be made in a straight road that the disturbance has varying, non-periodic values. Both of the simulations are implemented on the non-linear model.

4.5.1 Test Scenario 1

In Figure 4.14 the performance of the control systems in terms of yaw rate $\dot{\psi}$ and steering angle θ_s is presented. The $\mathcal{H}_\infty$ controller with the reduced states manages to minimize yaw rate, with less oscillations than the full-state $\mathcal{H}_\infty$ controller, while at the same time reaches a steady state in θ_s much faster than the rest of the controllers.

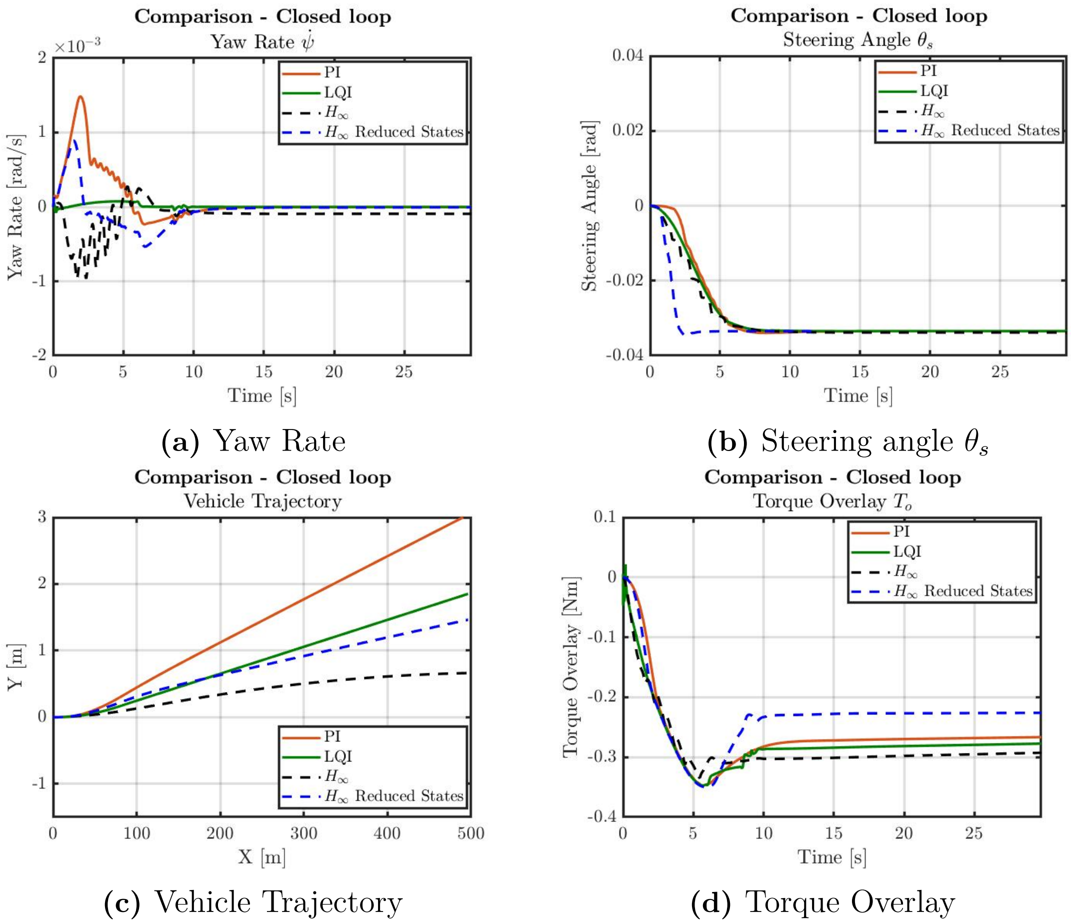

(a) Yaw Rate

(b) Steering angle θ_s

(c) Vehicle Trajectory

(d) Torque Overlay

Figure 4.14: Parameters of the closed loop non linear model for Test Scenario 1

Moreover, an estimation of the trajectory followed by the vehicle is presented in Figure 4.14c. Although the performance of the reduced $\mathcal{H}_\infty$ controller is not better than the full-state one, it is still sufficient since the car drifts around 1.5 meters in Y axis after a 500 meter straight path, which is better compared to the trajectory provided by the PI and LQI closed-loop systems.

As for the torque overlay, the output of the reduced-states $\mathcal{H}_\infty$ controller is smaller than the rest of the controllers, which indicates a potentially better utilization of the control torque required.

In Table 4.2 a comparison of the steady state values between the $\mathcal{H}_\infty$ and the $\mathcal{H}_\infty$ with reduced states controllers is presented. Yaw rate is reduced a bit more, which is expected as the full-state controller takes the β into account as well. The reason for that is because the full-state robust controller reduces first the yaw rate to an acceptable performance level and then tries to reduce the β. This makes the full-state more stable and easier to tune, but cannot reach the same performance to the yaw rate as the controllers that have it as the main. Keep in mind as well, tests with noisy or underperforming β sensors have not been made.

Parameter	$\mathcal{H}_\infty$	$\mathcal{H}_\infty$ **Reduced States**
$\dot{\psi}$ [rad/s]	-9.3×10^{-5}	-6.5×10^{-6}
θ_s [rad]	-3.38×10^{-2}	-3.34×10^{-2}
T_o [Nm]	-0.294	-0.226

Table 4.2: $\mathcal{H}_\infty$ Control strategy comparison

4.5.2 Test Scenario 2

Similarly to the previous scenario, the oscillations of the reduced-states $\mathcal{H}_\infty$ controller are much smaller compared to the full-state controller. However, the yaw rate is even smaller in the LQI closed-loop system. As for the steering angle, the performance of all the controllers is similar, as shown in Figure 4.15.

In Figure 4.15c, the estimated trajectory of the vehicle is showcased. The performance of the $\mathcal{H}_\infty$ controllers is similar, being more effective in reducing the drifting of the vehicle from its original lane, when comparing with the LQI and PI systems.

Finally, the additional torque provided by the EPS system to compensate the disturbances is shown in Figure 4.15d. The control output for all the cases is between the limits [-0.35, 0.35] Nm, satisfying the threshold of the electric motor for the extra torque boost.

4.6 Reference tracking

First, the linear model's reference capability is tested. A transfer function T_{ref} was added from T_h to $\dot{\psi}$. For the chosen W_r from eq. (3.30) and for added disturbance of 7 %, the plant's response is depicted on Fig 4.16. The resulting tracking is substantial, as the steady

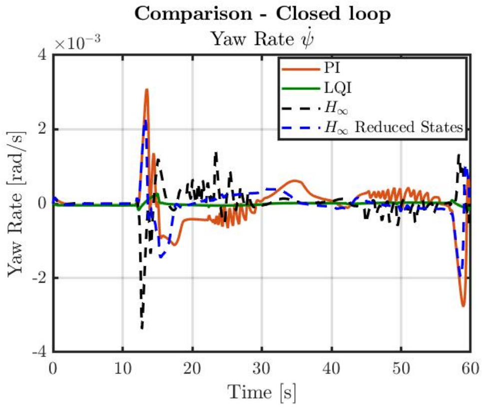

(a) Yaw Rate

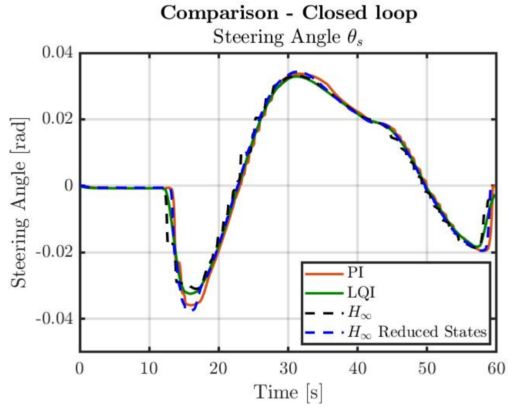

(b) Steering angle θ_s

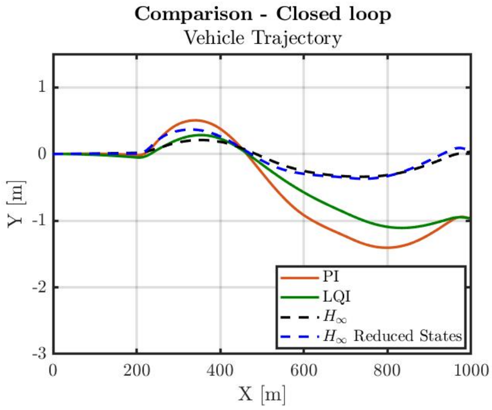

(c) Vehicle Trajectory

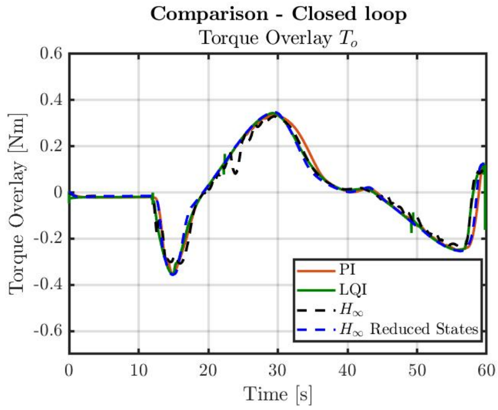

(d) Torque Overlay

Figure 4.15: Parameters of the closed loop non linear model for Test Scenario 2

state is met in a stable fashion. A phase time of about 0.25 s can be observed. These results shows the control logic's ability to not only reject the high induced disturbance, but also to follow the driver's order.

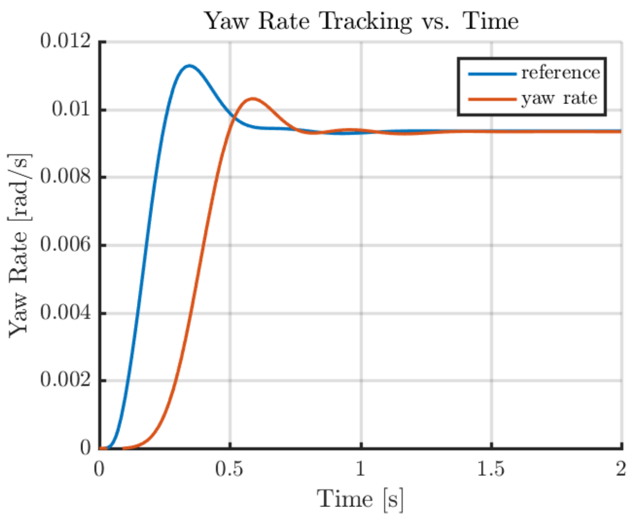

Figure 4.16: Reference Tracking Step Response - Linear Model

After developing the reference in the linear model, the capability of the controller to follow the reference is tested in CarMaker. In Figures 4.17-4.18, a comparison is made of the 2 models' behavior in reference tracking. The same driver torque input is given and the vehicle's response is captured. A first run was made in CarMaker to capture the yaw rate to be referenced, which was then fed to the controller. These two scenarios are the same as in section 4.1, a step of 3 Nm, and a sweep. It is fascinating to see that the yaw rate in the closed-loop system is even closer to the referenced one, but with a small phase delay. However, the signals for the side slip angle are again way different, indicating the big discrepancy in the measured and modeled values. Only the yaw rate and the side slip angle are shown, as the other states are linear and have a quite similar behavior to yaw rate, with the linear model with the controller being closer to the open loop-referenced run than the CarMaker one. In other words, although the idea based on the linear model is on the correct ground, the controller in CarMaker behaves differently. More tests were made with all the controllers for these reasons to become more obvious.

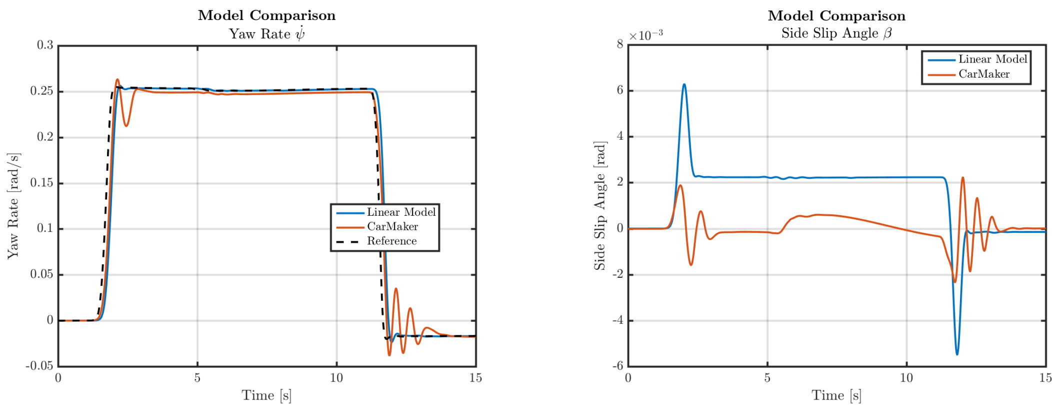

(a) Yaw Rate **(b)** Side Slip angle β

Figure 4.17: Reference Tracking: Step 3 Nm
CarMaker & Linear Model Closed-Loop Comparison

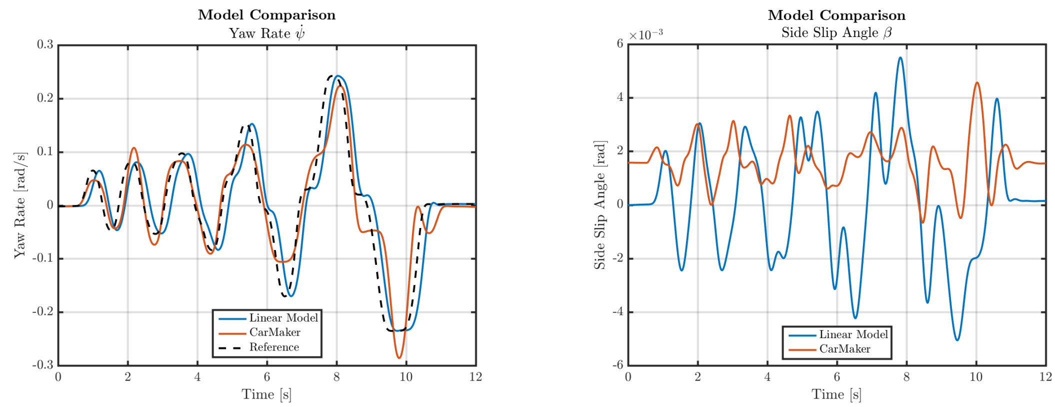

(a) Yaw Rate **(b)** Side Slip angle β

Figure 4.18: Reference Tracking: Sweep
CarMaker & Linear Model Closed-Loop Comparison

The first matter to be investigated, was how strict is the virtual driver, as he can be made to follow a specific path or set of actions, interfering with the output. For that, the same step was made, but with a reduced effort by the driver by 0.2 Nm, i.e. 2.8 Nm input, while the rest 0.2 are given by the motor. A disturbance lateral slope of 3 % was also given. The results for this test can be seen on Fig 4.19. All the controllers were tested, however the 1-DoF robust controllers did not perform very well; the 1-DoF with the reduced 3-states (denoted as '3s' in the figures) was omitted from the graphs because of that. The 2-DoF controllers on the other hand, both with the full states and with the reduced, performed much better. On the right side (Fig 4.19b), the torque overlay was added to show that the limits are met. The best behavior is met by the PI and 2-DoF $\mathcal{H}_\infty$. LQI is a bit slow, which is natural because of the integration part. Keep in mind though, that the step is still a bit fast; it is 3 Nm in 0.75 s, which in reality could be a lot slower. It was done so to test the controllers' limits.

For the next scenario, an ISO-double lane change (DLC) was tested. The exact scenario according to ISO can be seen in the Appendix. For this scenario also the driver was "relaxed". He was made to follow the path for the DLC but with an allowed path deviation of 0.2 m. A same disturbance of 3 % was also induced. The vehicle is driving at 90 kph. Such a manoeuvre in high velocity it is known to induce high dynamics and test the vehicle's handling limits. The vehicle's trajectory and the corresponding yaw rate can be seen on Fig 4.20. All the controllers were tested, though only the PI and $\mathcal{H}_\infty$ 2-DoF - full states, are shown, as they had the best performance. The 1-DoF ones made the vehicle unstable in most of the cases. The $\mathcal{H}_\infty$ 3s 2-DoF was also a bit off, which could be explained both because of the lack of dynamic states like the β, but also because of less tuning time. Again, this is a highly dynamic scenario, where the bicycle model loses its ability to capture some effects. However, the benefits of the $\mathcal{H}_\infty$ 2-DoF with all the states can be seen especially at the end of the manoeuvre, where the dynamic build-up made most of the controllers increase the yaw rate (Fig 4.20a) and lose it, than help the driver maintain the path.

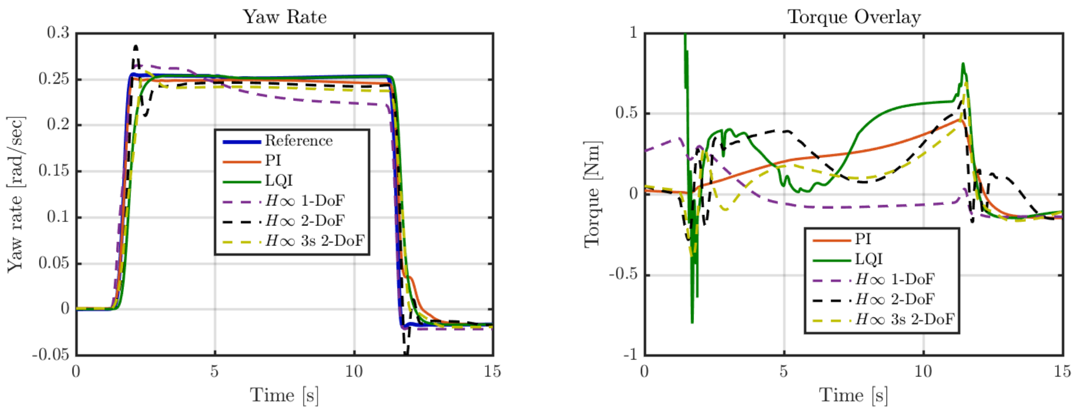

(a) Yaw Rate **(b)** Torque Overlay

Figure 4.19: Reference Tracking: Step 2.8 Nm
Controller Comparison in CarMaker

From the previous, there are several matters that need to be addressed. Firstly, the controller needs finer tuning. Especially, for the high dynamic scenarios, an increase of the controller's performance at higher frequencies makes the vehicle easier unstable. That is mainly due to the fact that the system with the EPS has a low natural frequency at about 2 Hz, and the addition of extra torque in that region is dangerous. This means, that it may actually not be possible to have a very good performance in higher frequencies

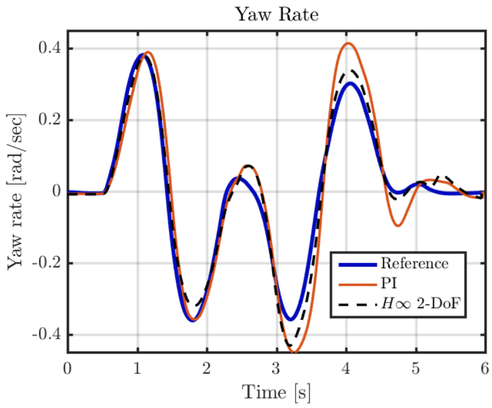

(a) Yaw Rate

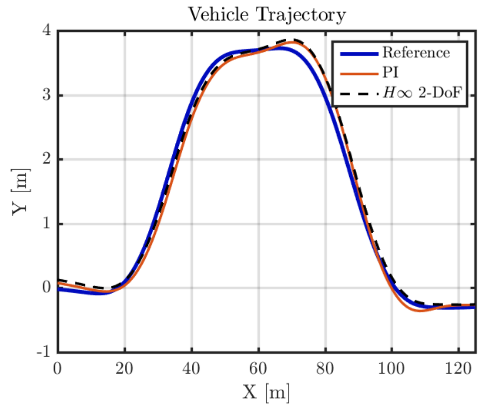

(b) Vehicle Trajectory

Figure 4.20: Reference Tracking: DLC
Controller Comparison in CarMaker

because of that reason. Secondly, to have a correct reference from the driver's torque input to the yaw rate is troublesome. It does not have a linear connection as both the motor's third order boost curve, and the non-linearities in the frictions, make the output both velocity and rate dependent.

4.7 Long Term Mitigation

A manoeuvre was made in CarMaker to test the algorithm. A 10 km straight road was designed, where the virtual driver is driving at 60 kph, with only purpose to stay within their lane. For this test, a sampling time of 0.5 s, and a sample size of 400 was used. That is, 200 seconds for T_{h0} to have its full value. In practice, a moving average was used, starting to give increasing values from 0 to 200 s, with the final value to be at that time. That is, because the estimation averages a number of zero values until reaching the 400 samples. It was chosen so, to have a gradual effect on the driver's behavior. As the motor is applying torque with an increasing value, the driver is also decreasing their effort. However, as the estimator is "looking" at the driver, the applied torque is also decreasing after some time. To avoid that, a hold in the averaging value was added some seconds later (see Fig 4.21b). Finally, the output T_{h0} was also tested for its statistical significance and for all tests, the conditions were met (null hypothesis). The sample size is big enough. In a real test though, it might need to be increased to gain the required significance.

The resulting behavior can be seen in Fig 4.21. The algorithm seems to be reducing the driver's effort to zero. Further tests at varying speeds show that this simple solution still performs well. In a real test scenarios, however, that may not always be the case, as the driver statistics at straight-line driving depend on external factors as well, such as road conditions. For instance, a long banked road would affect the average driver torque, and thus the average would be larger for a specific amount of time. With correct added functionality though, this algorithm should cover for most of the cases, as its foundation on the zero yaw rate approximation, is solid.

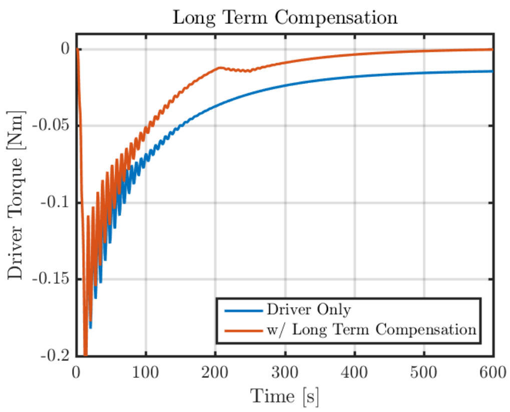

(a) Driver Torque before and after Compensation

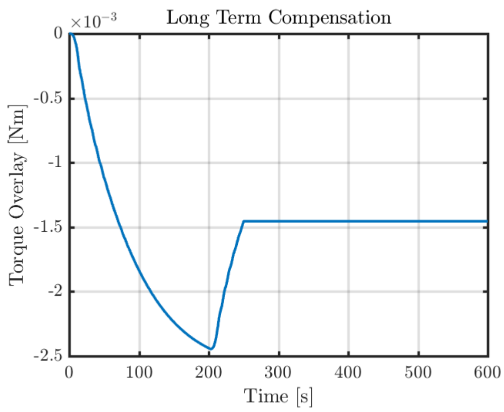

(b) Overlay Torque for the Compensation case

Figure 4.21: Compensation on Straight-line Driving

5

Conclusion

The linear 2-mass model developed has showed good qualities in both steady state and moderate dynamic scenarios. Its benefits come from its linear characteristics, which make for quickly obtained results and easy to implement for control purposes. Moreover, it gives a solid coupling of steering to vehicle dynamics, which is most usually either avoided or over-complicated. The main drawbacks of this model comes from each main subsystem. For the steering side the nonlinear, rate-dependent friction forces approximation to linearized ones, and for the vehicle dynamics side the velocity range dependency. However, it was shown that all tested controllers worked substantially well in the nonlinear environment of CarMaker, although they were tuned in a linear model, without such friction forces and for medium to high velocities. In the end, this is the range of approximation for this comfort feature and this model captures its behavior in a remarkable way.

Based on this model, several controllers were built with main goal to reject the unintentional torque. A comparison between these different controllers was presented for disturbance rejection and reference tracking.

Firstly, for disturbance rejection, the $\mathcal{H}_\infty$ controller was, without a doubt, the control strategy which performed best both in terms of compensating the error, as well as keeping the vehicle in its lane. The full state robust controller performed the best in terms of lane keeping. Including the side slip angle as a performance parameter gave easier tuning and more stability to the controller, however, a satisfactory reduction in that particular state was unattainable. Combined with the fact that the side slip angle is not easily measured, a reduced state controller was built, which focuses only on yaw rate. This controller provided acceptable results as well, still better than the rest of the controllers. Moreover, a better insight of the system behavior can be taken into consideration, proving robustness in different cases where the parameters may vary from the linear implementation.
Linear Quadratic Integral control has promising results as well, with minimizing yaw rate error with less oscillations due to the augmented state but is not as effective in lane keeping as the $\mathcal{H}_\infty$ controller. The Linear Quadratic Regulator is also promising in disturbance rejection, however its performance could be enhanced with more effective tuning to ensure that is able to compensate effectively different disturbance cases that may appear. In general, it was a challenging task to provide proper tuning for LQR to perform in both linear and non+linear model and for different scenarios.
The PI controller is easier to be implemented, since a linear model is not required. It can be applied immediately on the complex CarMaker simulation environment and can provide disturbance rejection, while tuning can be less time consuming since no design parameters should be defined. However, its lack of performance comparing to $\mathcal{H}_\infty$ and

LQI controllers, especially under uncertain assumptions, makes its choice questionable.

Secondly, by taking into account the reference signal while defining the LTI control system K, a 2-DoF reference tracking with robust performance and disturbance compensation was presented. The 2 Degree of Freedom, full-state, $\mathcal{H}_\infty$ controller has provided the best results in all the simulated scenarios regarding reference tracking.
The PI controller on the other hand, although it performs well in reference tracking, is not so effective in the combination of both following a reference and compensating the unintentional torques.
Linear Quadratic Integral control's performance in terms of reference tracking and mitigation of asymmetries is not as good as expected. The integration causes a delay in following the reference signal and its performance under disturbance at the same time is questionable. A different tuning approach could be followed, which was not implemented due to time limitations.
Finally, the 1 Degree of Freedom $\mathcal{H}_\infty$ controllers did not cope well in this case and pinpointed the importance of feeding the reference directly to the controller as an extra input.

In addition to the classical control techniques, a compensation technique based on statistics was presented, to cover for the long-term asymmetries. Straight-line drift can be accounted for, by first gathering driver torque data at zero yaw rate to perform an average estimation, and then apply this average value through the motor. Despite its simplicity, this approach has shown promising qualities reducing the driver's effort.

To sum up, the development of a 2-mass linear model, which captures adequately the dynamic behavior of the non linear model, was crucial for implementing effective control, model-based strategies. In general, the robust techniques might have a demanding way of tuning, but they can ensure robustness as they were the only controllers that once they were fine-tuned, they would perform well no matter the nature of the disturbance.

6

Future Work

Here, some insight on ways to improve the capabilities of the presented model and controller is given. Moreover, thoughts on possible expansion of this project are expressed as well.

Modelling:
Extremely dynamic cases would void the limits of the 2-mass model, mainly because of the rate dependency of the frictions and of the limitations of the bicycle model. As an expansion, nonlinear frictions could be added to increase model validity. In [27] for instance, there is an interesting way to include all the nonlinear friction forces in the motor's side, in a similar way as the rack's enhancement in this report. Moreover, a more advanced vehicle dynamics model could be utilized to increase the region of validity.

Disturbance Rejection:
It should be noted that a control to mitigate the effect of side winds was not investigated. In principle, the effect on the vehicle is known, so if the same solving procedure is followed as for the banking, it should not present big issues. In fact, the controller may already be able to compensate partly for low frequency side winds, since the banking compensation has a much larger impact and their effects are similar. Such a solution already exists in [28].

Reference Tracking:
During the reference tracking simulations, where the cases of step and lane changing were investigated, the focus was mostly on how would the closed loop system behave and if the extra torque boost is enough for the vehicle to follow the desired reference. Although the results are promising, this topic could be analyzed in more detail. Especially a correct connection between the driver's input and the wanted reference should be investigated more, because of the nonlinear motor connection to the same input.

Robust PI Control:
In general, a biased opinion is presented regarding the performance/implementation ratio. It is up to the user to decide which method fits their needs, and what should be sacrificed in order to choose a control strategy that satisfies them. PI controller is easier to be implemented, can be immediately applied and provide adequate results, but is not as effective as the $\mathcal{H}_\infty$ controllers in providing adequate disturbance rejection. A future implementation that combines the ready-to-go application of the PI controller and the robustness of the $\mathcal{H}_\infty$ controller is the robust PI controller. The main difference with the already used PI strategy is that the robust PI controller is using dynamical weights instead of proportional and integral terms, and it can have a better sense of the dynamical

changes of the system. It can also be properly tuned in the linear model first, capturing all the uncertainties that may arise, instead of blindly tuning directly on the complex non linear model. The controller was not presented in this thesis due to time limitations.

Driver Adaptation:
Additional tuning or a different control design could be included to provide a driver friendly feature that would be more sensitive on driver's reactions and more loose in terms of taking over the control of the vehicle in non critical situations. Good to notice as well is the fact that the robust controller only focuses on the frequency region specified, getting more adaptable, but also potentially solving known issues of the EPS about the steering feel. Moreover, since each driver's profile is different, it would be worth investigating driver specific adaptability. The rise in artificial intelligence (AI) use enables such investigations.

Bibliography

[1] Manfred Harrer and Peter Pfeffer. *Steering handbook*. Springer, 2017.

[2] Masato Abe. *Vehicle handling dynamics: theory and application*. Butterworth-Heinemann, 2015.

[3] Bosch. Servolectric®: Electric power steering systems for passenger cars. `https://www.bosch-mobility-solutions.com/en/products-and-services/passenger-cars-and-light-commercial-vehicles/steering-systems/electric-power-steering-systems/`. Accessed: 16.05.2019.

[4] S Grüner, A Gaedke, H Hsu, and M Harrer. The new epsapa in the porsche 911–innovative control concept for a sports car typical steering feel. *Chassis. tech plus, Munich, Germany*, 2012.

[5] Yijun Li, Taehyun Shim, Dexin Wang, and Timothy Offerle. Enhancement of steering feel of electric power assist steering system using modeling reference control. In *2018 Annual American Control Conference (ACC)*, pages 3257–3262. IEEE, 2018.

[6] American Association of State Highway and Transportation Officials. *A policy on geometric design of highways and streets*. 2011.

[7] Albin Gröndahl. Functional modelling and simulation of an electric power assisted steering. Master's thesis, Chalmers University of Technology, Gothenburg, Sweden, 2018.

[8] Ibrahim A Badiru. Assessment of the capability of eps to reduce steering wheel pull and vehicle misalignment. *SAE International Journal of Passenger Cars-Mechanical Systems*, 8(2015-01-1505):624–629, 2015.

[9] Richard M. Murray Karl Johan Aström. *Feedback Systems: An introduction for scientists and Engineers*. Princeton University Press, 12 April 2010.

[10] Michiel Hazewinkel. *Lagrange equations (in mechanics)*. Encyclopedia of Mathematics, Springer Science+Business Media B.V. / Kluwer Academic Publishers, 2001.

[11] Balazs Kulcsar. Linear control system design (ssy285) lecture notes, 2017. Automatic Control Group, Dept. of Signals and Systems, Chalmers University of Technology.

[12] D. Subbaram Naidu. *Optimal Control Systems*. CRC Press, 2002.

[13] O. Wingstrom. 3-dof helicopter laboratory session, 2014. Department of Signals and Systems,Chalmers University of Technology.

[14] Eric W. Weisstein. Frobenius norm. `http://mathworld.wolfram.com/FrobeniusNorm.html`. From MathWorld–A Wolfram Web Resource. Accessed 20.05.2019.

[15] I. C. Gohberg and M. G. Krein. *Introduction to the Theory of Linear Non-selfadjoint Operators*. American Mathematical Society, Providence, R.I., 1969.

[16] Balazs Kulcsar. Robust and nonlinear control design (ess076) lecture notes, 2018. Automatic Control Group, Dept. of Electrical Engineering, Chalmers University of Technology.

[17] Sigurd Skogestad and Ian Postlethwaite. *Multivariable feedback control: analysis and design*, volume 2. Wiley New York, 2007.

[18] DP Psoinos. *Statistics*. Ziti, Thessaloniki, 1999.

[19] Hans Pacejka. *Tire and vehicle dynamics*. Elsevier, 2005.

[20] Vivan Govender and Steffen Müller. Modelling and position control of an electric power steering system. *IFAC-PapersOnLine*, 49(11):312–318, 2016.

[21] Alaa Marouf, Chouki Sentouh, Mohamed Djemai, and Philippe Pudlo. Control of an electric power assisted steering system using reference model. In *2011 50th IEEE Conference on Decision and Control and European Control Conference*, pages 6684–6690. IEEE, 2011.

[22] Peter E Pfeffer, M Harrer, and DN Johnston. Interaction of vehicle and steering system regarding on-centre handling. *Vehicle System Dynamics*, 46(5):413–428, 2008.

[23] IPG Automotive. User's guide 7.0.1 carmaker®. Accessed: 16.05.2019.

[24] ureal(). `https://se.mathworks.com/help/robust/ref/ureal.html`. accessed 15.03.2019.

[25] Pongsathorn Raksincharoensak, Sato Daisuke, and Mathias Lidberg. Direct yaw moment control for enhancing handling quality of lightweight electric vehicles with large load-to-curb weight ratio. *Applied Sciences*, 9(6):1151, 2019.

[26] Masahiro Kubota, Masahiko Yoshizawa, and Hiroshi Mouri. An investigation of a steering-pull reduction method using the electric power steering system. Technical report, SAE Technical Paper, 2007.

[27] Steve Fankem, Thomas Weiskircher, and Steffen Müller. Model-based rack force estimation for electric power steering. *IFAC Proceedings Volumes*, 47(3):8469–8474, 2014.

[28] Said Mammar and Damien Koenig. Vehicle handling improvement by active steering. *Vehicle system dynamics*, 38(3):211–242, 2002.

[29] Bengt Jacobson. Vehicle dynamics compendium for course mmf062; edition 2018. Technical report, Chalmers University of Technology, 2018.

[30] Andrzej Reński. Identification of driver model parameters. *International Journal of occupational safety and ergonomics*, 7(1):79–92, 2001.

A

Appendix 1

A.1 Path Model

For a vehicle moving in the horizontal XY plane, its coordinates are described by (as seen in [29])

$$\begin{pmatrix} \dot{X} \\ \dot{Y} \end{pmatrix} = \begin{pmatrix} \cos\psi & -\sin\psi \\ \sin\psi & \cos\psi \end{pmatrix} \begin{pmatrix} u \\ v \end{pmatrix} \tag{A.1}$$

where X and Y is the earth-fixed coordinate system, and $[u, v]$ the velocities of the body-fixed coordinate system. Note that $u \approx V$ based on the steady state velocity linearization.

A.2 Double Lane Change: Extra Figure

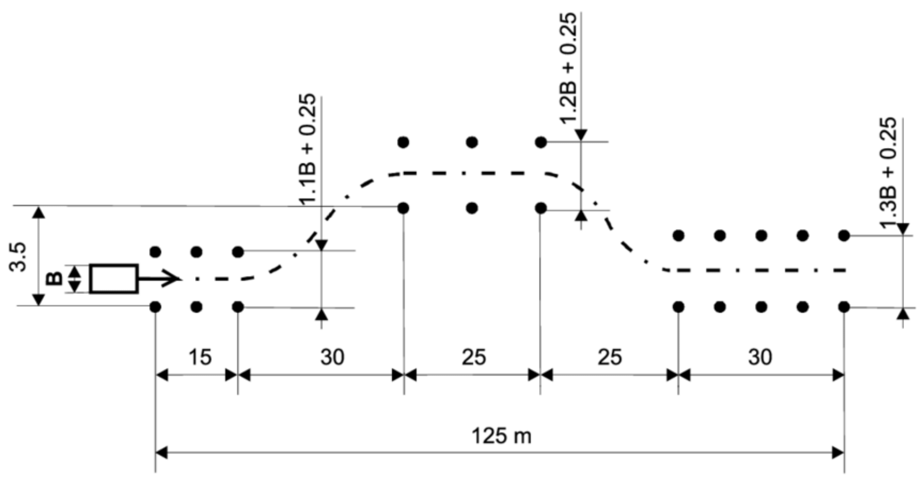

Figure A.1: The track of the double lane-change manoeuvre according to Standard No. ISO 3888:1975 (International Organization for Standardization [ISO], 1975); B-car width. Adopted from [30]